High-order harmonic generation and dynamic localization in a driven two-level system, a non-perturbative solution using the Floquet–Green formalism

2005 J. Phys. A: Math. Gen. 38 9979

(http://iopscience.iop.org/0305-4470/38/46/006)

INSTITUTE OF PHYSICS PUBLISHING JOURNAL OF PHYSICS A: MATHEMATICAL AND GENERAL

J. Phys. A: Math. Gen. **38** (2005) 9979–10005 doi:10.1088/0305-4470/38/46/006

High-order harmonic generation and dynamic localization in a driven two-level system, a non-perturbative solution using the Floquet–Green formalism

D F Martinez

Max-Planck-Institut für Physik komplexer Systeme, Nöthnitzer Straße 38, Dresden 01187, Germany

Received 27 July 2005, in final form 20 September 2005
Published 2 November 2005
Online at stacks.iop.org/JPhysA/38/9979

Abstract

Non-perturbative, exact analytical results are obtained for the harmonically driven two-level system with the use of a Floquet–Green operator formalism. From this operator, we find the quasi-energies and the Fourier components of the Floquet eigenstates which we use to construct the time-evolution operator of the system. As an application of our formalism, we study dynamic localization and high-order harmonic generation in this system. Our results show the existence of an initial condition that leads to an emission spectrum with only hyper-Raman lines for any frequency and strength of the driving field. We show the important role of the initial condition in determining the emission spectrum of this system. In the non-perturbative regime, the emission spectrum is found to be, in general, very sensitive to the amplitude of the driving field. We also derive an expression for the (coherent) emission spectrum which shows its dependence on the degree of localization of the system.

PACS numbers: 03.65.−w, 72.20.Ht, 42.65.Ky, 42.50.Ct

(Some figures in this article are in colour only in the electronic version)

1. Introduction

Harmonically driven systems have been traditionally studied in the field of atomic physics, regarding the interaction of electromagnetic radiation with matter. In particular, in the last two decades, there has been considerable interest in non-perturbative solutions to these systems, given the many new and interesting phenomena associated with intense optical field–matter interactions [1]. Also, in solid-state physics, there has been a significant amount of research on the effects of a periodic driving in the transport properties of nanostructures [2, 3] and also in relation to the problem of heat diffusion with time-dependent diffusivity [4].

Chief among those systems is the harmonically driven two-level system (HDTLS), which is a particularly important model in physics because of its simplicity and because it has proved to be very useful in describing many aspects of the interaction of matter with an electromagnetic field. The HDTLS has also been used to describe the electron dynamics in a double quantum well with an applied ac electric field [5]. It has also been used to describe an atom moving through a Fabry–Pérot cavity [6].

Despite its simple structure, exact analytical results valid in all of its parameter space are very hard to obtain, and therefore, most of the analytic results known are obtained using some approximation valid only within certain ranges of those parameters. In the field of atomic physics, this system was traditionally studied using the rotating wave approximation (RWA) [7], in which the 'counter-rotating' term of the harmonic driving is neglected. This approximation is valid near resonance and only for low intensities of the driving field. Presently, laser technology allows experimenters to produce very strong electromagnetic fields (short laser pulses) which can produce interesting non-linear effects in their interaction with matter.

For strong driving fields, the 'counter-rotating' term in the time-dependent part of the Hamiltonian does contribute significantly and, therefore, different theoretical approaches beyond RWA are required. One such method was first introduced by Autler and Townes [8]. Using Floquet's theorem and continued fractions, they derived a general solution in order to investigate the effect of a radio frequency field on the l-type microwave absorption line of the doublet $J = 2 \rightarrow 1$ of the molecules of gaseous OCS.

Later, Shirley [9] employed Floquet theory to reduce the solution of a periodic time-dependent Hamiltonian to the problem of diagonalization of a time-independent matrix. This matrix was then used to calculate eigenvalues and transition probabilities for a HDTLS system and also to derive higher order (beyond linear RWA) analytic approximations valid in the case of weak driving. Later approaches to this problem, usually within the context of a spin system in a magnetic and a rf field, have involved the use of continued fractions [10–12], although the role played by Floquet theory in those approaches (and in particular the role of the quasi-energy) is not clear.

A different kind of analytical expression for the quasi-energy of the HDTLS, which does not involve continued fractions, was reported by Zhao [13]. It makes use of group theoretical arguments for its derivation and involves the evaluation of complicated infinite sums. Apart from its intrinsic theoretical value, this solution does not provide a practical way to study this system.

There have been a variety of approaches used to obtain approximate analytic expressions. Most of them have been obtained in the high frequency limit [14–16], for $\omega \gg \omega_0$, or in the strong field limit [17, 18], for $v \gg \hbar\omega$. Here ω is the frequency of the driving, ω_0 is the energy difference between the two levels of the unperturbed Hamiltonian and v is the strength of the driving.

One of the most interesting features of this system, which was found in those perturbative solutions, is that, at some specific values of the driving field strength (the zeros of the zeroth-order Bessel function), dynamic localization (DL) occurs. In the context of quantum wells this means that, despite a nonzero tunnelling probability between the two wells, a system initially prepared in one of them will remain there indefinitely. DL in quantum wells was first studied by Großmann *et al* [5]. In an earlier work [19], a manifestation of DL was found in a tight binding potential with an applied ac electric field.

In a paper by Ivanov [20] in which high-order harmonic generation (HHG) by diatomic molecular ions is considered, and then more recently in works by Santana *et al* [21] and also Delgado and Gomez Llorente [22], analytical expressions in terms of Bessel functions were

found, valid in the (perturbative) regime where DL occurs. This regime can be characterized by the condition $\omega_0/\omega \ll 1$ for any v, or $\omega_0/\omega \ll \sqrt{v/\hbar\omega} \gg 1$. We will say that whenever any of these two conditions is satisfied, the system is in the DL regime, where, as expected, our results converge to the known Bessel-function expressions.

Our goal in this work is two-fold. First, to present a fully developed Floquet–Green formalism for harmonically driven systems, which is suitable for the complete solution of any such system without any approximations. The calculation of such Floquet–Green function plays a major role in the solution of many problems where a periodic time dependence in the potential is present, as it is the case, for instance, in quantum-driven transport [3]. Our second goal is to show how this formalism can be applied in a concrete system; in this work, we consider the important case of a HDTLS and give an exact solution valid in all of its parameter range. This exact solution is expressed in terms of continued fractions, suitable to the study of the regime where neither the RWA nor any other perturbative approach works. Our aim is to present a whole picture of this system, of its eigenvalues and eigenstates in the different regions of its parameter space and to obtain, from our exact solution, some new results regarding the two main features of this system, namely DL and HHG.

In section 2, we derive the Floquet–Green operator formalism and establish a connection between the poles of this operator and the quasi-energies and components of the Floquet eigenstates. In section 3, we apply this formalism to the specific case of the HDTLS. There, we obtain an expression for the quasi-energies which makes use of continued fractions. We also derive the Floquet eigenstates of the system and study their dependence on the amplitude of the driving field for different values of the two-level energy difference. The time-evolution operator is then constructed using these eigenstates. We devote section 4 to the study of DL, and in section 5 we derive some expressions for HHG in this system. Finally, in section 6, we summarize our findings and give some concluding remarks.

2. Floquet–Green operator for harmonic driving

The pioneering work of Shirley [9], Zel'dovich [23] and Sambe [24] laid down the theoretical foundations for a complete treatment of time-periodic potentials, based on the same mathematical tools already developed for time-independent potentials. Of significant importance among these tools is the Green function, whose definition and application for time-periodic systems have not been clear until recently. A Floquet–Green function method for the solution of radiative electron scattering in a strong laser field was introduced by Faisal [25]. In this section, we develop the complete Floquet–Green operator formalism for general harmonically driven Hamiltonians that was introduced by the author in a previous work [26].

We start by considering a general Hamiltonian of the general form

$$H(t) = H_0 + 2V\cos(\omega t), \tag{1}$$

where H_0 and V are Hermitian operators in the Hilbert space ($\mathcal{H}$) of the system. Because of the periodicity of the Hamiltonian, according to Floquet's theorem, the solutions to Schrödinger's equation $\mathrm{i}\hbar\frac{\partial}{\partial t}|\Psi(t)\rangle = H(x,t)|\Psi(t)\rangle$ are of the form

$$|\Psi^e(t)\rangle = \mathrm{e}^{-\mathrm{i}et/\hbar}|\phi^e(t)\rangle, \tag{2}$$

where $|\phi^e(t)\rangle = \left|\phi^e\left(t+\frac{2\pi}{\omega}\right)\right\rangle$.

Inserting this into Schrödinger's equation, one arrives at the eigenvalue equation

$$H^F(t)|\phi^e(t)\rangle = e|\phi^e(t)\rangle, \tag{3}$$

where $H^F(t)$ is defined as

$$H^F(t) \equiv H(t) - i\hbar\frac{\partial}{\partial t}. \tag{4}$$

As pointed out by Sambe [24], since equation (3) is an eigenvalue equation, it can be solved using the standard techniques developed for time-independent Hamiltonians, provided we extend the Hilbert space to include the space of time-periodic functions. In this extended space, the time parameter can be treated as another degree of freedom of the system. A similar concept is used in classical mechanics and gives rise to the concept of a 'half' degree of freedom when dealing with time-dependent Hamiltonians.

A suitable basis for this extended Hilbert space ($\mathcal{R}$) is $\{|\alpha\rangle \otimes |n\rangle, \ldots\}$, where $\{|\alpha\rangle, \ldots\}$ is a basis for the Hilbert space $\mathcal{H}$ of the system, and we define $\langle t|n\rangle = e^{-in\omega t}$, with n integer. Clearly $\{|n\rangle, \ldots\}$ spans the vector space ($\mathcal{T}$) of periodic functions, and therefore $\mathcal{R} = \mathcal{H} \bigotimes \mathcal{T}$. In this basis, equation (3) becomes a matrix eigenvalue equation of infinite dimension with an infinite number of eigenvalues. It is not difficult to prove that if e_i is an eigenvalue, with corresponding eigenvector $|\phi^{e_i}(t)\rangle$, then $e_i + m$ is also an eigenvalue (all quantities are assumed to be in units of $\hbar\omega$), with corresponding eigenvector $|\phi^{e_i+m}(t)\rangle = e^{im\omega t}|\phi^{e_i}(t)\rangle$. Accordingly, the eigenstate corresponding to eigenvalue $e_i + m$ has the same structure as the eigenstate corresponding to e_i, except that it is displaced by m on the energy axis. Because of this, to find all the eigenvectors and eigenvalues of the Floquet Hamiltonian one needs only to consider $-\frac{1}{2} \leqslant e < \frac{1}{2}$. We will use the symbol ε to refer to the Floquet eigenvalues restricted to this interval and call them 'quasi-energies'. Clearly, any Floquet eigenvalue e_i can be written as $e_i = \varepsilon_i + p$ for some $-\frac{1}{2} \leqslant \varepsilon_i < \frac{1}{2}$ and some integer p. It can be shown that, in general, there are N distinct quasi-energies (except for accidental degeneracies) if the Hilbert space $\mathcal{H}$ is N dimensional.

This periodic structure in the eigenvalues does not mean that the 'replica' eigenstates have no relevance; they are also valid solutions of equation (3) and are essential for completeness in the extended Hilbert space $\mathcal{R}$ [27]. They also allow us to understand some features of the quasi-energies of the system in terms of avoided crossings between 'replica' eigenstates.

The Floquet–Green operator for the Floquet Hamiltonian in equation (3) is defined by the equation (see [26])

$$[\mathbb{1}E - H^F(t')]\mathcal{G}(E, t', t'') = \mathbb{1}\delta_\tau(t' - t''), \tag{5}$$

where $\delta_\tau(t)$ is the τ-periodic delta function $\left(\tau = \frac{2\pi}{\omega}\right)$.

In terms of the complete (infinite) set $\{|\phi^{e_i}(t)\rangle\}$ of eigenfunctions of the Floquet Hamiltonian (equation (4)), the solution for equation (5) is

$$\mathcal{G}(E, t', t'') = \sum_i \frac{|\phi^{e_i}(t')\rangle\langle\phi^{e_i}(t'')|}{E - e_i}. \tag{6}$$

From the previous discussion about the eigenvalues and eigenfunctions of the Floquet Hamiltonian, we can write the Floquet–Green operator entirely in terms of the eigenfunctions corresponding to values e_i between $-\frac{1}{2}$ and $\frac{1}{2}$. We will denote these eigenvalues as ε_γ. Using this, the Floquet–Green operator can be written as

$$\mathcal{G}(E, t', t'') = \sum_\gamma \sum_p e^{ip\omega(t'-t'')} \frac{|\phi^{\varepsilon_\gamma}(t')\rangle\langle\phi^{\varepsilon_\gamma}(t'')|}{E - \varepsilon_\gamma - p}, \tag{7}$$

where $\gamma = 1, \ldots, N$ for $\mathcal{H}$ being N dimensional and $p = -\infty, \ldots, \infty$.

Operating on both sides of this equation with $\frac{1}{\tau^2}\int_0^\tau \int_0^\tau e^{im\omega t'} e^{-in\omega t''}\, dt''\, dt'$, we obtain

$$\mathcal{G}_{m,n}(E) = \sum_{\gamma,p} \frac{1}{E - \varepsilon_\gamma - p} \left|\phi^{\varepsilon_\gamma}_{m+p}\right\rangle\left\langle\phi^{\varepsilon_\gamma}_{n+p}\right|, \tag{8}$$

where

$$\mathcal{G}_{m,n}(E) = \frac{1}{\tau^2}\int_0^\tau \int_0^\tau \mathrm{e}^{\mathrm{i}m\omega t'}\,\mathrm{e}^{-\mathrm{i}n\omega t''}\mathcal{G}(E,t',t'')\,\mathrm{d}t''\,\mathrm{d}t'$$

and

$$\left|\phi_m^{\varepsilon_\gamma}\right\rangle = \frac{1}{\tau}\int_0^\tau \mathrm{e}^{\mathrm{i}m\omega t'}|\phi^\varepsilon(t')\rangle\,\mathrm{d}t'. \tag{9}$$

For $m = n = 0$,

$$\mathcal{G}_{0,0}(E) = \sum_{\gamma,p}\frac{1}{E-\varepsilon_\gamma - p}\left|\phi_p^{\varepsilon_\gamma}\right\rangle\left\langle\phi_p^{\varepsilon_\gamma}\right|. \tag{10}$$

This last equation shows us the relationship between the residue of the operator $\mathcal{G}_{0,0}(E)$ at the pole $\varepsilon_\gamma + p$ and the Fourier component $\left|\phi_p^{\varepsilon_\gamma}\right\rangle$ of the Floquet eigenstate $|\phi^{\varepsilon_\gamma}(t)\rangle$. Note that $|\phi^{\varepsilon_\gamma}(t)\rangle = \sum_p \mathrm{e}^{-\mathrm{i}p\omega t}\left|\phi_p^{\varepsilon_\gamma}\right\rangle$. From this we conclude that, *corresponding to each pole at $E = \varepsilon_\gamma + p$ of the Floquet–Green operator $\mathcal{G}_{0,0}(E)$, there is an oscillating term of the form $\mathrm{e}^{-\mathrm{i}p\omega t}$ in the Floquet eigenstate specified by the quasi-energy ε_γ.*

Let us go back to the task of finding an explicit solution to the Floquet–Green operator in equation (5). Applying $\frac{1}{\tau^2}\int_0^\tau\int_0^\tau \mathrm{e}^{\mathrm{i}m\omega t'}\,\mathrm{e}^{-\mathrm{i}n\omega t''}\,\mathrm{d}t''\,\mathrm{d}t'$ on both sides of this equation and using equation (4) together with the above definitions, we get

$$[\mathbb{1}(E+m) - H_0]\mathcal{G}_{m,n} - V(\mathcal{G}_{m+1,n} + \mathcal{G}_{m-1,n}) = \mathbb{1}\delta_{m,n}. \tag{11}$$

The explicit solution of this equation, in terms of matrix continued fractions, was derived in [26]. The resulting expression for the operator $\mathcal{G}_{0,0}(E)$ is

$$\mathcal{G}_{0,0}(E) = (\mathbb{1}E - H_0 - V_{\mathrm{eff}}(E))^{-1}, \tag{12}$$

where

$$V_{\mathrm{eff}}(E) = V_{\mathrm{eff}}^{+}(E) + V_{\mathrm{eff}}^{-}(E),$$

with

$$V_{\mathrm{eff}}^{\pm}(E) = V\cfrac{1}{\mathbb{1}(E\pm 1) - H_0 - V\cfrac{1}{\mathbb{1}(E\pm 2) - H_0 - V\cfrac{1}{\vdots}V}V}. \tag{13}$$

A related method for the solution of equation (11) was used in [28].

The convergence of matrix continued fractions is a difficult mathematical subject which is still under development. Regarding this issue, we can mention that convergence has always been achieved in all our numerical calculations, and that, for each specific type of system, the number of terms needed to assure the convergence of the matrix continued fractions in equation (13) is a particular function of the strength V of the driving field. For some systems we found this dependence to be linear (e.g. HDTLS), for others it is approximately quadratic (e.g. scattering by an oscillating δ-function potential [29]).

We will now specialize these results for the case of a two-state system driven by a classical single-frequency potential.

3. Harmonically driven two-level system

In this section, we apply the formalism previously presented to the case of a driven two-level system of the form

$$H = \frac{\tilde{\omega}_0}{2}\sigma_z + 2v\cos(\omega t)\sigma_x, \tag{14}$$

where H, $\tilde{\omega}_0$ and v are given in units of $\hbar\omega$. In the context of an electron interacting with an electric field, the amplitude $2v$ corresponds to the (static) dipole moment of the electron times the applied electric field, i.e. $2v = \mu E_0/\hbar\omega$ (the factor of 2 has been introduced for convenience), and the classical electric field is of the form $E(t) = E_0\cos(\omega t)$. In a double quantum-dot realization of this Hamiltonian, the non-driven part, $\frac{\tilde{\omega}_0}{2}\sigma_z$, describes the tunnelling between the states localized on each dot, $\{|1\rangle, |2\rangle\}$. This tunnelling gives rise to a splitting of $\hbar\omega_0 = \tilde{\omega}_0\hbar\omega$ between the energy levels $-\frac{\hbar\omega_0}{2}, +\frac{\hbar\omega_0}{2}$, whose corresponding eigenstates we denote by $\{|a\rangle, |b\rangle\}$, and where $|b\rangle = \frac{1}{\sqrt{2}}(|1\rangle + |2\rangle)$ and $|a\rangle = \frac{1}{\sqrt{2}}(|1\rangle - |2\rangle)$. The Hamiltonian in equation (14) is written in the basis $\{|a\rangle, |b\rangle\}$. For an atomic system, $\frac{\tilde{\omega}_0}{2}\sigma_z$ describes two bound states of the atomic (or molecular) potential, or, in the context of ionizing systems, it could also be thought of as describing a bound state and the continuum [30, 31]. An electron moving in a Fabry–Pérot cavity [6] or a 1/2 spin system with an applied magnetic and microwave field [10–12] are also examples of systems where this model has been used.

We emphasize here that, even though this system has been studied many times in the past, both numerically and analytically, most of the analytic results have been derived using approximations that are valid in a certain range of parameters in which the particular perturbative approach used works. In this work, we will derive new exact analytical expressions for the quasi-energies and Floquet eigenstates of the system, which we will use to study DL and HHG in this system.

Our approach will make use of continued fractions, which have been used before to study this system, especially in the context of spin 1/2 systems in a magnetic and a rf field, starting with the seminal work of Autler and Townes [8]. Also, in a previous treatment of this problem, the time-dependent Green function and continued fractions were used, although outside of the frame of the Floquet formalism [32].

To find the exact solution to this Hamiltonian we need to evaluate equations (12) and (13), for the case $V = v\sigma_x$ and $H_0 = \frac{\omega_0}{2}\sigma_z$. It can be checked easily that, given the off-diagonal form of V and the diagonal form of H_0, the matrices $V^{\pm}_{\text{eff}}(E)$ are diagonal. Its diagonal components will be denoted, respectively, by $\left\{v^{\pm}_a(E), v^{\pm}_b(E)\right\}$. The dynamic effective potential $V_{\text{eff}}(E)$ is therefore also diagonal and of the form

$$V_{\text{eff}}(E) = \begin{bmatrix} v^+_a(E) + v^-_a(E) & 0 \\ 0 & v^+_b(E) + v^-_b(E) \end{bmatrix}. \tag{15}$$

The $v^{\pm}_{a/b}$ functions are given by the following coupled recursive relations:

$$v^{\pm}_a(E) = \frac{v^2}{E \pm 1 - \frac{\tilde{\omega}_0}{2} - v^{\pm}_b(E \pm 1)}, \qquad v^{\pm}_b(E) = \frac{v^2}{E \pm 1 + \frac{\tilde{\omega}_0}{2} - v^{\pm}_a(E \pm 1)}. \tag{16}$$

Replacing $v^{\pm}_a$ into $v^{\pm}_b$ (and vice versa), we obtain the decoupled recursive relations

$$\begin{aligned} v^{\pm}_a(E) &= \frac{v^2}{E \pm 1 - \frac{\tilde{\omega}_0}{2} - \dfrac{v^2}{E \pm 2 + \frac{\tilde{\omega}_0}{2} - v^+_a(E \pm 2)}}, \\ v^{\pm}_b(E) &= \frac{v^2}{E \pm 1 + \frac{\tilde{\omega}_0}{2} - \dfrac{v^2}{E \pm 2 - \frac{\tilde{\omega}_0}{2} - v^+_b(E \pm 2)}}. \end{aligned} \tag{17}$$

From equation (12), the solution for $\mathcal{G}_{0,0}(E)$ is also a diagonal matrix of the form

$$\mathcal{G}_{0,0}(E) = \begin{bmatrix} g^a(E) & 0 \\ 0 & g^b(E) \end{bmatrix}, \tag{18}$$

with

$$g^a(E) = \frac{1}{E + \dfrac{\tilde{\omega}_0}{2} - v_a^+(E) - v_a^-(E)},$$
$$g^b(E) = \frac{1}{E - \dfrac{\tilde{\omega}_0}{2} - v_b^+(E) - v_b^-(E)}. \tag{19}$$

For this system, the minimum number of steps (m) necessary to obtain convergence of the continued fractions in equation (17) was found to obey $m = 2v + 2$.

It can easily be seen from equation (17) that this system possesses the symmetry $v_a^{\pm}(-E) = -v_b^{\mp}(E)$, which from equation (19) gives us $g_a(-E) = -g_b(E)$. This means that to find the two quasi-energies of the system one only has to look for a pole in either $g_a(E)$ or $g_b(E)$ in the range $-0.5 \leqslant E \leqslant 0.5$; the other pole is symmetrically located on the opposite side of the (quasi) energy axis.

3.1. Poles of $\mathcal{G}_{0,0}(E)$ and the quasi-energies of the system

As discussed before, the quasi-energies of the system can be obtained from the poles in $g_a(E)$ and $g_b(E)$. We showed that it is sufficient to study the poles in only one of these functions since for any pole in $g_a(E)$ at $E = E^*$ there is a corresponding pole in $g_b(E)$ at $E = -E^*$. This implies the existence of two quasi-energies in the system, $\varepsilon, -\varepsilon$. The quasi-energy ε can be obtained from the solution to $g_b(E)^{-1} = 0$ in the interval $-0.5 < E < 0.5$. From equations (17) and (19), the poles of $g_b(E)$ satisfy the equation

$$\delta = \cfrac{v^2}{\tilde{\omega}_0 - \cfrac{v^2}{\delta+2 - \cfrac{v^2}{\delta+3+\tilde{\omega}_0 - \cfrac{v^2}{\delta+4 - \cfrac{v^2}{\vdots}}}}} + \cfrac{v^2}{\delta-1+\tilde{\omega}_0 - \cfrac{v^2}{\delta-2 - \cfrac{v^2}{\delta-3+\tilde{\omega}_0 - \cfrac{v^2}{\delta-4 - \cfrac{v^2}{\vdots}}}}}, \tag{20}$$

where $\delta = E - \frac{\tilde{\omega}_0}{2}$. The quasi-energy is obtained as $\varepsilon = \left(\frac{\tilde{\omega}_0}{2} + \delta\right) \bmod 1$.

In figure 1, we show one of the quasi-energies of the system, for different values of $\tilde{\omega}_0$. These functions are plotted as a function of the driving strength v. We have included the resonant case $\tilde{\omega}_0 = 1$ and several values in the high-frequency regime where $\tilde{\omega}_0 < 1$. In the limit where $\tilde{\omega}_0 \ll \max(1, \sqrt{v})$, we have $\varepsilon(v) \approx \frac{\tilde{\omega}_0}{2} J_0(4v)$. This result was first obtained by Shirley [9]. It is precisely in this regime where it was shown [21, 22] that DL appears as a dominant feature. As $\tilde{\omega}_0$ decreases, we observe a very quick convergence to the approximate result $\varepsilon(v) \approx \frac{\tilde{\omega}_0}{2} J_0(4v)$. Already for $\tilde{\omega}_0 = 0.25$, the difference between the exact result for $\varepsilon(v)$ and the approximation cannot be observed at the scale of the graph. For $\tilde{\omega}_0 = 0.1$, we plotted both $\varepsilon(v)$ and $-\varepsilon(v)$ to make the location of the zeros of $J_0(4v)$ more visible. As we can also see in figure 2, increasing $\tilde{\omega}_0$ always displaces the zeros of $\varepsilon(v)$ towards smaller values. This behaviour was also observed by Villas-Bôas *et al* [33] in the case of a double quantum well with an intense ac electric field and an applied magnetic field. Note also that, as it is easy to derive analytically, the only case where the initial slope of the quasi-energy is not zero is the resonant case.

In figure 2, we show the quasi-energy as a function of the driving strength v, for low frequencies, where $\tilde{\omega}_0 \geqslant 1$. The resonant case is included for comparison. Also, the dotted

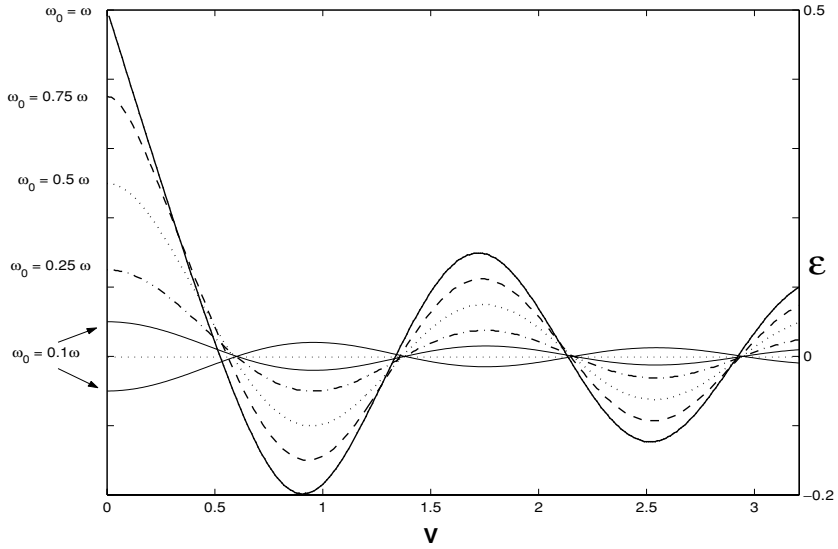

Figure 1. Quasi-energy as a function of driving amplitude (v), for different values of $\tilde{\omega}_0 \equiv \omega_0/\omega \leqslant 1$ (high frequencies).

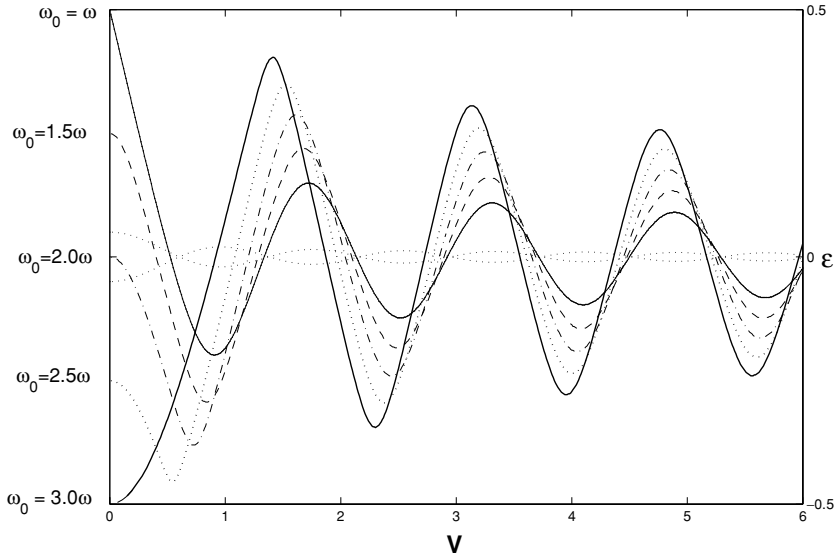

Figure 2. Quasi-energy as a function of driving amplitude, for different values of $\tilde{\omega}_0 \geqslant 1$ (low frequencies). The functions $\pm 0.05 J_0(4v)$ are plotted with dotted lines for comparison.

line shows the functions $\pm 0.05 J_0(4v)$ in order to indicate the location of the zeros of this Bessel function. For lower frequencies (increasing $\tilde{\omega}_0$), the amplitude and sharpness of the oscillations around $\varepsilon = 0$ increase, the location of the zeros shifts to the left and the parabola that describes (except in the resonant case) the initial behaviour of the curve opens up. For

$\tilde{\omega}_0 \gtrsim 2$, one can get from equation (20) that the initial behaviour of the quasi-energy is parabolic and has the form

$$\delta(v) \approx \frac{2\tilde{\omega}_0}{\tilde{\omega}_0^2 - 1} v^2. \tag{21}$$

This remains a good approximation for all values of v until $\delta(v) \approx \frac{\tilde{\omega}_0 - 1}{4}$ and provided $\epsilon(v)$ does not reach the edges of the Brillouin zone $(-0.5, 0.5)$ before that. If it does so, then the quasi-energy experiences an avoided crossing, whose sharpness is proportional to $\tilde{\omega}_0$ and decreases with the value of v at which the anti-crossing occurs.

3.2. Components of the Floquet eigenstates

In the previous subsection, we showed how to obtain the diagonal part of the Floquet–Green operator and discussed its poles, from which the quasi-energies of the system can be obtained. In this part, we study the Floquet eigenstates and their general behaviour as the amplitude of the driving field changes. In the appendix, we show that they can be written in the form

$$|\phi^{-\varepsilon}(t)\rangle = K(t)|a\rangle + Z(t)|b\rangle$$

and

$$|\phi^{\varepsilon}(t)\rangle = -Z(t)^*|a\rangle + K(t)^*|b\rangle, \tag{22}$$

with

$$\begin{aligned} K(t) &= N\left[\sum_{n=-\infty}^{\infty} \mathrm{e}^{-2\mathrm{i}n\omega t} K_{2n}(-\varepsilon)\right], \\ Z(t) &= N\left[\sum_{n=-\infty}^{\infty} \mathrm{e}^{-\mathrm{i}(2n-1)\omega t} Z_{2n-1}(-\varepsilon)\right]. \end{aligned} \tag{23}$$

N is a normalization constant and $|K(t)|^2 + |Z(t)|^2 = 1$. In equation (A.10) of the appendix, we also show the explicit form of the components K_{2n}, Z_{2n+1}. It can be seen there that all components K_{2n} and Z_{2n-1} are real, and therefore $K(0)$ and $Z(0)$ are real numbers.

In figure 3, we show the components of one of the Floquet eigenstates of the system, $|\phi^{\varepsilon}(t)\rangle$, for the resonant case and for eight different values of the driving field amplitude. In the upper figure of each panel, we show the quantities Z_n, K_n (with n odd for Z_n and n even for K_n), and in the lower panels we show the quantities $\ln|Z_n|$, $\ln|K_n|$.

A notable qualitative difference between the behaviour of Z_{2n-1} and K_{2n} is the fact that for stronger values of v, the former becomes more antisymmetric while the last one becomes more symmetrical around $n = 0$. We will comment shortly about the consequence that this has for the dynamic localization of the system. The fact that the eigenstates of the system have components that are harmonics of the driving field frequency ω, translates, as we will study in the next section, into a (coherent) emission spectrum of the system which contains also many frequencies. The possibility of exciting a system at a particular frequency with a strong field and producing radiation that includes frequencies much higher than the driving frequency (in some cases hundreds of times bigger) is called high-order harmonic generation (HHG) and has been studied in many experiments [1]. HHG of a driven two-level system has been studied in the past and it has been shown [15, 20, 30, 34–37] that there is a plateau in the spectrum followed by a sharp cut-off after which the amplitudes of the harmonics decrease exponentially. In the section dedicated to HHG, we will provide new results regarding this phenomenon in HDTLS.

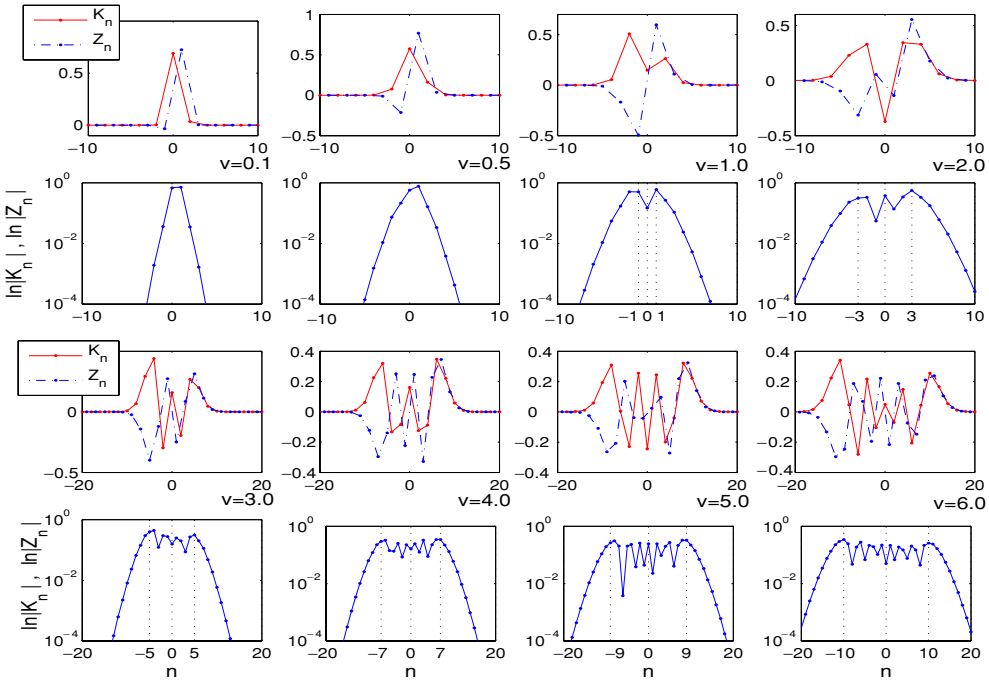

Figure 3. Components of the Floquet eigenstates for $\tilde{\omega}_0 = 1$ and for eight different values of the driving amplitude. The logarithmic plots show the 'plateau' structure of these eigenstates, which gives rise to the well-known plateau studied in HHG. The cut-off location (N_e) follows the approximate rule $N_e = 2v - 1$.

As one can see directly from figure 3, in most of the cases shown, the Floquet eigenstates show a particular structure with two clearly distinguishable regions. The first region which, in a non-rigorous way, we call the 'irregular' one can be described as corresponding to the Floquet components with $|n| \lesssim N_e = 2v - 1$ (in the resonant case this is valid if $v \geqslant 1$). The amplitude of these Floquet components depends strongly on n and v, and there are frequent sign changes. This gives rise to the 'plateau' region typical in HHG. The second region, or the 'regular' one, corresponds to the components with $|n| > N_e$, and it is characterized by having amplitudes that decay exponentially with n. Also note that the components K_n and Z_n do not change sign in that region, with $K_{2n} > 0$ and $\mathrm{sg}(Z_{2n-1}) = \mathrm{sg}(n)$ ($\mathrm{sg}(x) \equiv x/|x|$). For other values of $\tilde{\omega}_0$, a plateau region was always found whenever $v \gtrsim \sqrt{\tilde{\omega}_0}$ (for $\tilde{\omega}_0 \geqslant 1$), in agreement with a similar expression obtained by Kaplan [30] in the limit $\tilde{\omega}_0 \gg 1$. For $\tilde{\omega}_0 < 1$, the plateau forms for any $v \gtrsim 1$.

A practical comment, derived from the above results, is that the infinite sums in equations (23) can be replaced by finite sums with upper and lower limits given by $\pm 4v$. This gives a total number of Floquet components for each eigenstate of the order of $8v$. This clearly means that, if one were to use the Floquet Hamiltonian matrix defined in equation (4) to directly compute the Floquet eigenstates, the minimum required size for that matrix would be $(16v) \times (16v)$. From this result it could be argued, from a numerical point of view, that our method should be numerically superior to the diagonalization of the Floquet Hamiltonian (diagonalization is a time-consuming matrix operation). These considerations are, however, of no practical importance in the present case since for a system as simple as the HDTLS, there are no computational difficulties when using any method for any realistic value of the

driving potential (in fact, numerical integration of Schrödinger's equation is probably the fastest method). The importance of our approach is determined by the fact that it provides us with analytical expressions from which a deeper understanding of the dynamics can be obtained.

The expression $N_e = 2v - 1$, as we will see later, would give a cut-off in the HHG plateau at $N_{\rm cut} = 2N_e = 4v - 2$, which differs by two harmonics with the standard result $N_{\rm cut} = 4v$ found in the previous work [20]. The difference is not significant since our 'cut-off' refers to the position of the harmonic after which there is a monotonic decrease in the strength of the harmonics, whereas in [20] the cut-off refers to the location of the last harmonic with a significant amplitude. Clearly, this last location should be a few harmonics higher than our value.

We now provide a simple derivation of our result, by first looking at the conditions to obtain for $n > 0$ a perfectly flat, triple plateau in the components of the Floquet eigenstates. This means that we will assume $K_{n+2} = Z_{n+1} = K_n$ (which gives three consecutive components with the same amplitude), for some n even. This condition can be achieved if, from equation (A.10), $v_a^+(\varepsilon + n) = v_b^+(\varepsilon + n + 1) = v$. From equation (16) we get the condition

$$n = 2v - 1 + \frac{\tilde{\omega}_0}{2} - \varepsilon.$$

If instead, we had chosen the triple plateau to be of the form $Z_{n+2} = K_{n+1} = Z_n$ (for n odd), then the equation for n would be

$$n = 2v - 1 - \frac{\tilde{\omega}_0}{2} - \varepsilon.$$

If we now apply the same reasoning for a triple cusp to occur in the negative energy components, beginning at the component $-n$, we get the conditions (for n odd and even, respectively)

$$n = 2v - 1 + \frac{\tilde{\omega}_0}{2} + \varepsilon, \qquad n = 2v - 1 - \frac{\tilde{\omega}_0}{2} + \varepsilon.$$

Clearly, since in general these four equations cannot be (nor we care for them to be) satisfied simultaneously, we instead look for a condition that will produce a simple (possibly) double cusp, *both* at N_e and $-N_e$. This would describe the location of the two broad peaks that are, in all cases, at the limit between the 'irregular' and the 'regular' region. For obtaining this symmetric flat cusp condition, we pick the equation that is right in the middle of the set of four equations given above. This equation is clearly

$$N_e = 2v - 1, \tag{24}$$

with the nice property that the ε and the $\tilde{\omega}_0$ dependence drops out. This is a result that should work well whenever there is a well-defined 'plateau' region, that is, for $v \geqslant \sqrt{\tilde{\omega}_0}$ when $\tilde{\omega}_0 \geqslant 1$, or $v \geqslant 1$ when $\tilde{\omega}_0 < 1$. As can be seen in figure 3, for $\tilde{\omega}_0 = 1$ and $v \geqslant 1$, this equation seems to describe well the location of the peaks in the spectrum of an eigenstate that separate the plateau from the exponential decay region. For other values of $\tilde{\omega}_0$, it also gives good agreement with the data.

To investigate further the structure of the Floquet eigenstates of this system, we use equation (22), and evaluate at $t = 0$,

$$\begin{aligned} |\phi^{-\varepsilon}(0)\rangle &= \cos\theta|a\rangle + \sin\theta|b\rangle, \\ |\phi^{\varepsilon}(0)\rangle &= -\sin\theta|a\rangle + \cos\theta|b\rangle, \end{aligned} \tag{25}$$

where, using $K(0)^2 + Z(0)^2 = 1$, we have defined the angle θ so that $K(0) = \cos\theta$ and $Z(0) = \sin\theta$.

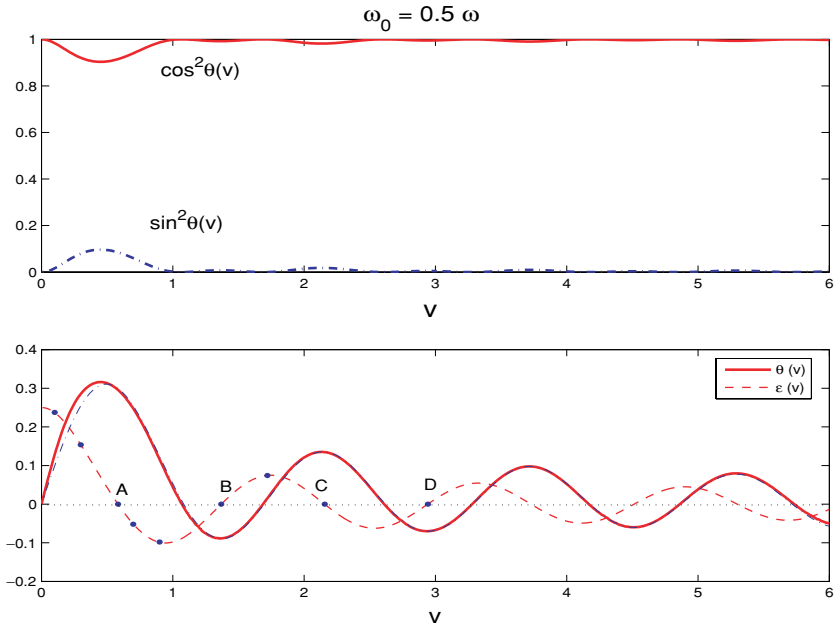

Figure 4. The upper panel shows the functions $\cos^2(\theta(v))$ and $\sin^2(\theta(v))$, for $\tilde{\omega}_0 = 0.5$. At $t = 0$, one of the Floquet eigenstates is given by $|\phi^{-\varepsilon}(0)\rangle = \cos\theta(v)|a\rangle + \sin\theta(v)|b\rangle$. The lower panel shows the functions $\theta(v)$ (solid line) and $\varepsilon(v)$ (dashed line). The dash-dotted line corresponds to the Struve function $\tilde{\omega}_0 \frac{\pi}{4} H_0(4v)$. Points A, B, C and D correspond to the values of v for which DL occurs.

We now concentrate on the study of the quantities $\cos\theta(v)$, $\sin\theta(v)$, $\theta(v)$, which, as we will see in the next sections, play an important part in the evolution of the system, and correspondingly in the dynamical localization and harmonic generation of the system. In the following, we will study them for two different values of the parameter $\tilde{\omega}_0$: driving frequency above resonance, for $\tilde{\omega}_0 = 0.5$, and driving frequency below resonance, for $\tilde{\omega}_0 = 2$.

In figures 4 and 5, we show the results for $\tilde{\omega}_0 = 0.5$ and $\tilde{\omega}_0 = 2.0$, respectively. The upper panels show the dependence of the functions $\cos^2(\theta(v))$ and $\sin^2(\theta(v))$, and the lower panels the functions $\theta(v)$ and $\varepsilon(v)$. As a function of the driving field amplitude v, these functions show an oscillatory behaviour, which can be better appreciated in the lower panels, where the function $\theta(v)$ is plotted alongside with $\varepsilon(v)$. An interesting feature of these functions is the fact that in general, and to a good approximation, there seems to be a phase shift of $\approx\pi/2$ between $\varepsilon(v)$ and $\theta(v)$, which corresponds to a distance of $\Delta v \approx 0.4$ between their maxima. This means that to (almost) every maxima of $\theta(v)$ corresponds a zero of $\varepsilon(v)$ (the DL points) and vice versa, with the only exceptions occurring at the first maxima or the first zero of these functions. Note also that $\theta(v)$ does not oscillate symmetrically around zero, with the clear consequence that the peaks in the functions $\cos^2(\theta(v))$ and $\sin^2(\theta(v))$ have uneven heights, with alternating high and low peaks, although with an overall decrease in height. This alternating pattern of maxima seems to be a general feature of the system, which we have found for all the values of $\tilde{\omega}_0$ that we examined.

The DL regime, which can be characterized by the parameter $\alpha' \equiv \tilde{\omega}_0 \min(1, 1/\sqrt{v}) \ll 1$, has been studied in several works. In this regime, the eigenstates of the system [15, 21] were

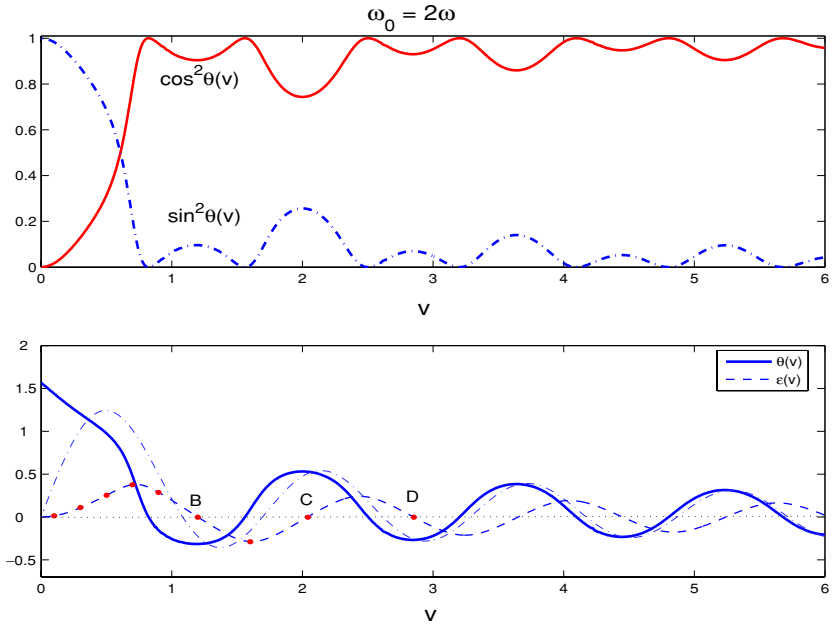

Figure 5. Same as in figure 4. Low-frequency case, $\tilde{\omega}_0 = 2$.

found to be, at $t = 0$, of the form

$$\begin{aligned} |\phi^{-\varepsilon}(0)\rangle &= |a\rangle + \tilde{\omega}_0 \frac{\pi}{4} H_0(4v)|b\rangle, \\ |\phi^{\varepsilon}(0)\rangle &= -\tilde{\omega}_0 \frac{\pi}{4} H_0(4v)|a\rangle + |b\rangle, \end{aligned} \tag{26}$$

where $H_0(4v)$ is the Struve function [38] defined as

$$H_0(4v) \equiv \frac{4}{\pi} \sum_{n=0}^{\infty} \frac{J_{2n+1}(4v)}{2n+1}. \tag{27}$$

In the lower panels in figures 4 and 5, we have plotted using a dash-dotted line the function $\tilde{\omega}_0 \frac{\pi}{4} H_0(4v)$. As it was expected, since in the DL regime $\sin\theta \ll 1$, then $\sin\theta \approx \theta$, and therefore $\theta(v) \to \tilde{\omega}_0 \frac{\pi}{4} H_0(4v)$. The convergence of $\theta(v)$ to the Struve function is clearly slower for bigger values of $\tilde{\omega}_0$. It is however rather remarkable that this function seems to approximate well the function $\theta(v)$ much before the DL regime ($\alpha' \ll 1$) is reached. For $\tilde{\omega}_0 = 0.5$ and $v = 1$, which gives $\alpha' = 0.5 \lesssim 1$, we already see a good agreement between those two functions. One can also see from figures 4 and 5 that the Struve function, even in the low-frequency case ($\tilde{\omega}_0 = 2$), correctly gives the height of the maxima in $\theta(v)$, with the difference between those two functions being mostly a phase difference that tends to zero as $v \to \infty$. From the asymptotic form of the Struve function in the limit $v \to \infty$, we obtain

$$\theta(v) \sim \tilde{\omega}_0 \frac{\pi}{4} \sqrt{\frac{1}{2\pi v}} \sin(4v - \pi/4) \approx \alpha \sin(4v - \pi/4) \qquad \text{for} \quad v \to \infty, \tag{28}$$

where we defined $\alpha \equiv \sqrt{\pi/32}\alpha' = \sqrt{\pi/32}\,\frac{\tilde{\omega}_0}{\sqrt{v}}$, for $v > 1$. From now on we call α the 'DL parameter'. Equation (28) establishes a nice connection between the DL parameter and the amplitude of the oscillations in the function $\theta(v)$.

3.3. Time-evolution operator

To find out the time evolution of an initial state of the form $|a\rangle$ or $|b\rangle$, we can use the eigenstates at time $t = 0$, as given by equation (25). From that equation we can express $|a\rangle$ and $|b\rangle$ in the form

$$\begin{aligned} |a\rangle &= \cos\theta|\phi^{-\varepsilon}(0)\rangle - \sin\theta|\phi^{\varepsilon}(0)\rangle, \\ |b\rangle &= \sin\theta|\phi^{-\varepsilon}(0)\rangle + \cos\theta|\phi^{\varepsilon}(0)\rangle. \end{aligned} \tag{29}$$

From these, it is now straightforward to construct two orthogonal solutions to Schrödinger's equation which, at $t = 0$, correspond to each one of the eigenstates of H_0:

$$|a(t)\rangle = \mathrm{e}^{\mathrm{i}\varepsilon t}\cos\theta|\phi^{-\varepsilon}(t)\rangle - \mathrm{e}^{-\mathrm{i}\varepsilon t}\sin\theta|\phi^{\varepsilon}(t)\rangle$$

and

$$|b(t)\rangle = \mathrm{e}^{\mathrm{i}\varepsilon t}\sin\theta|\phi^{-\varepsilon}(t)\rangle + \mathrm{e}^{-\mathrm{i}\varepsilon t}\cos\theta|\phi^{\varepsilon}(t)\rangle, \tag{30}$$

where $|a(0)\rangle = |a\rangle$ and $|b(0)\rangle = |b\rangle$. Using equation (22) into above expressions, we get

$$|a(t)\rangle = [\cos\theta K(t)\,\mathrm{e}^{\mathrm{i}\varepsilon t} + \sin\theta Z^*(t)\,\mathrm{e}^{-\mathrm{i}\varepsilon t}]|a\rangle + [\cos\theta Z(t)\,\mathrm{e}^{\mathrm{i}\varepsilon t} - \sin\theta K^*(t)\,\mathrm{e}^{-\mathrm{i}\varepsilon t}]|b\rangle$$

and

$$|b(t)\rangle = [\sin\theta K(t)\,\mathrm{e}^{\mathrm{i}\varepsilon t} - \cos\theta Z^*(t)\,\mathrm{e}^{-\mathrm{i}\varepsilon t}]|a\rangle + [\sin\theta Z(t)\,\mathrm{e}^{\mathrm{i}\varepsilon t} + \cos\theta K^*(t)\,\mathrm{e}^{-\mathrm{i}\varepsilon t}]|b\rangle. \tag{31}$$

The time-evolution operator for this system, which is defined by the equation $|\Psi(t)\rangle = U(t,0)\|\Psi(0)\rangle$, can be extracted, in the basis $\{|a\rangle, |b\rangle\}$, directly from the above expressions

$$U_{ab}(t,0) = \begin{bmatrix} u_{aa}(t) & -u_{ba}^*(t) \\ u_{ba}(t) & u_{aa}^*(t) \end{bmatrix}, \tag{32}$$

where

$$\begin{aligned} u_{aa}(t) &= \cos\theta K(t)\,\mathrm{e}^{\mathrm{i}\varepsilon t} + \sin\theta Z^*(t)\,\mathrm{e}^{-\mathrm{i}\varepsilon t}, \\ u_{ba}(t) &= \cos\theta Z(t)\,\mathrm{e}^{\mathrm{i}\varepsilon t} - \sin\theta K^*(t)\,\mathrm{e}^{-\mathrm{i}\varepsilon t}. \end{aligned} \tag{33}$$

The subindex ab in U_{ab} is there to remind us of the basis used to represent the time-evolution operator.

Another way to arrive at the same result is by making use of the general expression (equation (27) in [39])

$$U(t,0) = \Phi(t)\,\mathrm{e}^{-\mathrm{i}\Lambda t}\Phi^{-1}(0), \tag{34}$$

where the columns of the Floquet matrix $\Phi(t)$ are the components of the Floquet eigenstates of the system and Λ is a diagonal matrix whose components are the quasi-energies. For our system, from equation (22), the Floquet matrix is

$$\Phi(t) = \begin{bmatrix} K(t) & -Z^*(t) \\ Z(t) & K^*(t) \end{bmatrix} \tag{35}$$

and $\Lambda = -\varepsilon\sigma_z$.

4. Dynamic localization

It is interesting to study the situation where the system's initial state is a superposition of the eigenstates of H_0. In particular, and in the context of quantum wells, a particularly interesting initial state is one in which the electron is localized in one of the wells. Such an initial state corresponds to $|\Psi(0)\rangle = |1\rangle \equiv \frac{1}{\sqrt{2}}(|a\rangle + |b\rangle)$ or $|\Psi(0)\rangle = |2\rangle \equiv \frac{1}{\sqrt{2}}(|a\rangle - |b\rangle)$. In this case, we are interested in calculating the probability to find the system at that same location

after a time t. The solution can be found by applying the transformation $V = \frac{1}{\sqrt{2}}(\sigma_z + \sigma_x)$, which corresponds to the change of basis $\{|a\rangle, |b\rangle\} \rightarrow \{|1\rangle, |2\rangle\}$, to the evolution matrix in equation (32). The resulting matrix, $U_{12} = V U_{ab} V^{-1}$, can be written as

$$U_{12}(t, 0) = \begin{bmatrix} u_{11}(t) & -u_{21}^*(t) \\ u_{21}(t) & u_{11}^*(t) \end{bmatrix}, \tag{36}$$

with

$$\begin{aligned} u_{11} &= \mathrm{Re}(u_{aa}) + \mathrm{i}\,\mathrm{Im}(u_{ba}), \\ u_{21} &= \mathrm{Re}(u_{ba}) - \mathrm{i}\,\mathrm{Im}(u_{aa}). \end{aligned} \tag{37}$$

It is a well-known fact that DL occurs only at the points where the quasi-energies vanish, i.e. $\varepsilon(v) = 0$ (we will refer to these particular values of the amplitude v as the DL points). At these particular values of driving field amplitude v, as it can be seen from equations (32) and (33), the dynamics of the system becomes strictly periodic, with period $2\pi/\omega$, for any initial condition. The points where $\sin\theta(v) = 0$ also produce a periodic evolution of the system (except for an overall time-dependent phase factor), but only for the particular initial conditions $|\Psi(0)\rangle = |a\rangle$ or $|\Psi(0)\rangle = |b\rangle$.

To study the system at the DL points, we will look at the quantity $|u_{11}(t)|^2$, which gives the probability that the system, if localized in a well (e.g. $|1\rangle$) at time $t = 0$, would remain in that well at a later time t. For $\varepsilon(v) = 0$ and from equations (33) and (37), we get

$$u_{1,1}(t) = \cos\theta[\mathrm{Re}(K(t)) + \mathrm{i}\,\mathrm{Im}(Z(t))] + \sin\theta[\mathrm{Re}(Z(t)) + \mathrm{i}\,\mathrm{Im}(K(t))], \qquad \text{at DL points.} \tag{38}$$

Since this probability is periodic, $u_{1,1}(0) = u_{1,1}(2\pi/\omega) = 1$, it is interesting to see what is the value of this function half-way through a cycle of the field, that is, for $\omega t = \pi$. From equation (A.9) we can deduce that $K(\pi/\omega) = K(0) = \cos\theta$ and $Z(\pi/\omega) = -Z(0) = -\sin\theta$. Using this, we get from the above equation

$$u_{1,1}(\pi/\omega) = \cos\theta^2 - \sin\theta^2 = \cos(2\theta), \qquad \text{at DL points.} \tag{39}$$

We will show in the following figures that the function $\cos(2\theta)$ plays an important role in quantifying the localization of the system at the DL points.

In the lower panels of figures 4 and 5, we have placed dots on the quasi-energy functions $\varepsilon(v)$, at different values of v. In the upper panels in figures 6 and 7, we show, for each one of those points, the corresponding probability $|u_{1,1}(t)|^2$, as given by equations (33) and (37). This probability gives the location of the particle, as a function of time, when starting from the initial state $|1\rangle$. In figure 6, we study the case $\tilde{\omega}_0 = 0.5$. In this plot, one can see that the probability evolves in a manner that is similar to the high-frequency regime which has been studied in the literature. The function can be described as being of the form $\cos(\varepsilon t)$ + small time-periodic oscillations. Clearly, at the DL points (A, B, C, D), when $\varepsilon = 0$, the probability is exactly periodic (period $2\pi/\omega$) and oscillates between 1 and a value that depends on the driving field amplitude v and $\tilde{\omega}_0$. As derived before, in the middle of the driving period, the probability $|u_{1,1}|^2 = \cos^2(2\theta(v))$.

Given the correspondence between the maxima of $\theta(v)$ and the zeros of $\varepsilon(v)$, we can conclude that the minima of the function $\cos^2(2\theta(v))$ tell us the value of the probability $|u_{1,1}(t)|^2$ half-way through the driving field period ($t = \pi/\omega$), at the corresponding DL point (with the exception of point A). This value of $|u_{1,1}(t)|^2$ is very important because it gives us information about the extent to which the particle is localized when the DL points are reached. As we can see in the lower panels of figures 6 and 7, when the function $|u_{1,1}(t)|^2$ has a local minimum at $t = \pi/\omega$, then $\cos^2(2\theta(v))$ is close to the absolute minimum value that $|u_{1,1}(t)|^2$ reaches throughout a whole period, $P_l = \min(|u_{1,1}(t)|^2)$. It is therefore an

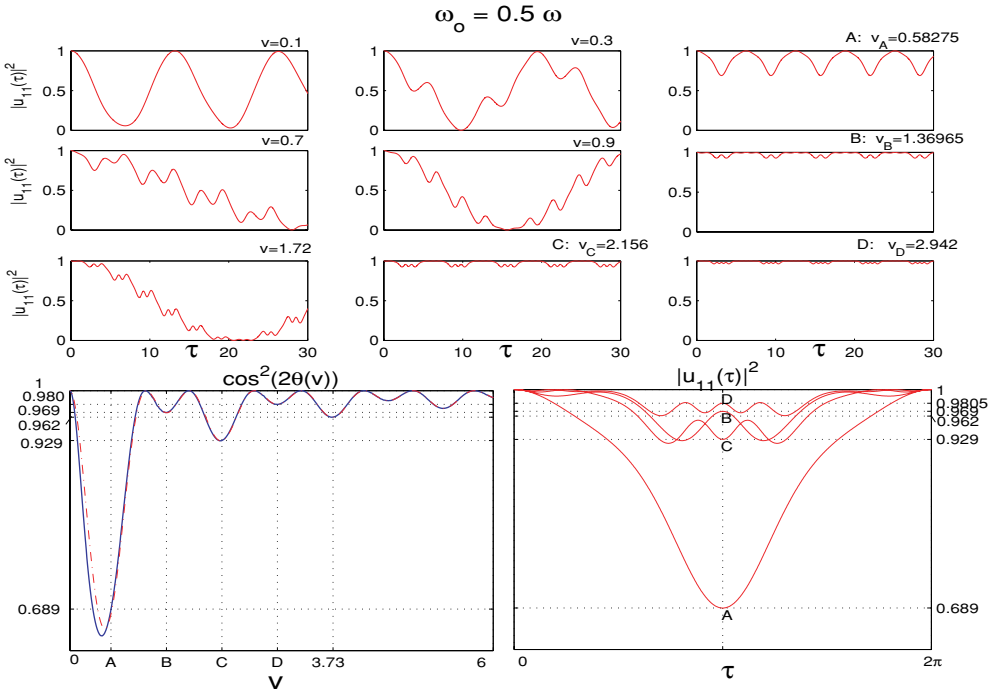

Figure 6. The probability to remain in the initial state $|1\rangle$ as a function of time ($\tau = \omega t$), for nine different values of the driving amplitude and for $\tilde{\omega}_0 = 0.5$. The lower panels show that the function $\cos^2(2\theta(v))$, at the DL points (A, B, C, D), gives a good approximation to the amount of localization P_l in this system. $P_l = \min(|u_{11}(\tau)|^2)$. In the lower-left panel, the function $\cos^2(2\tilde{\omega}_0 \frac{\pi}{4} H_0(4v))$ is shown with a dash-dotted line for comparison.

important number for describing the amount of localization in the system. When the function $|u_{1,1}(t)|^2$ has a local maximum at $t = \pi/\omega$, then $\cos^2(2\theta(v))$ is still equal to that value but this is not necessarily close to P_l (especially when we are far from the DL regime). This is the case at points B and D in those figures. Surprisingly, however, P_l, for cases B and D, is given, to a good approximation, by the value of the function $\cos^2(2\theta(v))$ at the minima that corresponds to the *next* DL point. We do not know why this should be so but it was found to be the case in all the cases that we examined. According to this, the DL points can be grouped in pairs, with (B, C) having a similar amount of localization, given by $\cos^2(2\theta(v_c))$, points (D, E) with a localization given by $\cos^2(2\theta(v_E))$, and so on. It is therefore the deeper minima in $\cos^2(2\theta(v))$ that give us directly the amount of localization in the system.

An interesting question to ask, because of practical applications, is whether there is a simple relationship between the amount of localization P_l, $\tilde{\omega}_0$ and v. In other words, given a particular amount of localization P_l, and a given $\tilde{\omega}_0$, what is the required driving field amplitude for the system to achieve such level of localization? To answer this question in the DL regime (where we expect a high level of localization, $P_l \lesssim 1$), one can use equation (28) to derive an approximate relationship between P_l, $\tilde{\omega}_0$ and v. At the maxima of $\theta(v)$ (DL points), $\theta(v) \sim \alpha$, which gives $P_l = \cos^2(2\theta) \approx 1 - 4\theta^2 = 1 - \frac{\pi}{8}\frac{\tilde{\omega}_0^2}{v}$, from which one finally gets

$$v \approx \frac{\pi \tilde{\omega}_0^2}{8(1 - P_l)}. \tag{40}$$

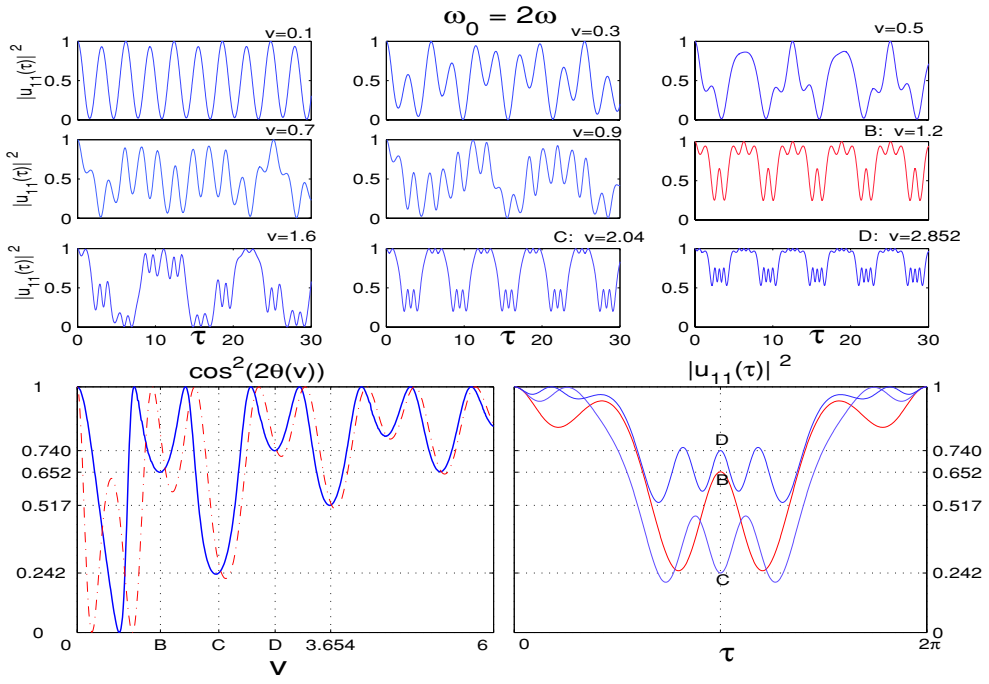

Figure 7. As in figure 6. Low-frequency case, $\tilde{\omega}_0 = 2$.

A remarkable feature of this simple equation, which has been derived assuming $v > 1, \alpha \ll 1$, is that it already gives good results even for a localization as low as $P_l = 0.5$, with the accuracy improving further for higher values of P_l. For $P_l = 0.5$ the result is $v \sim 0.78\tilde{\omega}_0^2$, for $P_l = 0.9$ one obtains $v \sim 4\tilde{\omega}_0^2$ and for $P_l = 0.99$ it gives $v \sim 40\tilde{\omega}_0^2$. It is interesting to compare equation (40) with the results obtained for the localization of a two-level system driven by a square wave [40].

5. High-order harmonic generation

A two-level model can be an accurate representation of the dynamics in an atom in a laser field, provided that all other atomic levels are weakly coupled to the radiation and do not affect the dynamics significantly. In very strong fields, this is likely not to be the case; however, the HDTLS is an important idealization which helps understand basic concepts and phenomena present in more complicate systems. In this section, we will use our previous results and derive an exact and previously unknown expression for the expected value of the dipole moment of this system, in which there is an explicit dependence on the initial state and on the other parameters of the problem.

The expected value of the dipole moment of the system can be calculated from the expression

$$\langle d(t)\rangle = \langle \Psi(t)|X|\Psi(t)\rangle = \mu\langle \Psi(0)|\sigma_x(t)|\Psi(0)\rangle, \tag{41}$$

where

$$\sigma_x(t) \equiv U_{ab}(t)^{\dagger}\sigma_x U_{ab}(t), \tag{42}$$

and using equations (32), we get

$$\sigma_x(t) = \begin{bmatrix} \mathrm{Re}[u^*_{aa}(t)u_{ba}(t)] & \left[u^2_{aa}(t) - u^2_{ba}(t)\right]^* \\ u^2_{aa}(t) - u^2_{ba}(t) & -\mathrm{Re}[u^*_{aa}(t)u_{ba}(t)] \end{bmatrix}. \tag{43}$$

For a general initial condition of the form $|\Psi(0)\rangle = c_a|a\rangle + c_b|b\rangle$, we get

$$\langle d(t)\rangle/\mu = \mathrm{Re}[u^*_{aa}(t)u_{ba}(t)](|c_a|^2 - |c_b|^2) + 2\,\mathrm{Re}\left[c_a c_b^* \left(u^2_{aa}(t) - u^2_{ba}(t)\right)\right]. \tag{44}$$

If we now define the following time-periodic functions:

$$\begin{aligned} R(t) &\equiv \mathrm{Re}(K(t))\,\mathrm{Re}(Z(t)) + \mathrm{Im}(K(t))\,\mathrm{Im}(Z(t)) && \text{(odd harmonics)}, \\ Q(t) &\equiv \mathrm{Re}(K(t))\,\mathrm{Im}(K(t)) - \mathrm{Re}(Z(t))\,\mathrm{Im}(Z(t)) && \text{(even harmonics)}, \\ P(t) &\equiv \mathrm{Im}(K(t))^2 + \mathrm{Re}(Z(t))^2 && \text{(even harmonics)}, \end{aligned} \tag{45}$$

then, using this, and plugging equations (33) into equation (44), we obtain (after some lengthy algebra) the final expression

$$\begin{aligned} \langle d(t)\rangle/\mu = {} & [-\sin(2\theta)\cos(2\epsilon t) + 2\cos(2\theta)R(t) + 2\sin(2\theta)\sin(2\epsilon t)Q(t) \\ & + 2\sin(2\theta)\cos(2\epsilon t)P(t)](|c_a|^2 - |c_b|^2) \\ & + [\cos(2\theta)\cos(2\epsilon t) + 2\sin(2\theta)R(t) - 2\cos(2\theta)\sin(2\epsilon t)Q(t) \\ & - 2\cos(2\theta)\cos(2\epsilon t)P(t)]\,\mathrm{Re}(2c_a c_b^*) \\ & + [-\sin(2\epsilon t) - 2\cos(2\epsilon t)Q(t) + 2\sin(2\epsilon t)P(t)]\,\mathrm{Im}(2c_a c_b^*). \end{aligned} \tag{46}$$

The quantities θ, ε, $P(t)$, $Q(t)$, $R(t)$ depend on v, even though we do not explicitly indicate so in this notation. Following the terminology in [15], we will refer to the case $|c_a| = 1$ or $|c_b| = 1$ (and therefore $c_a c_b^* = 0$) as the 'optical' initial condition (OIC), to the case $c_a = \pm c_b$ as the 'tunnelling' initial condition (TIC) and to the case $c_a = \pm \mathrm{i} c_b$ as the 'complex tunnelling' initial condition (CTIN).

From the expectation value of the dipole moment, one can obtain the (coherent) emission spectrum of the system from the expression $|d(\Omega)|^2 = \left|\frac{1}{T}\int_{t_0}^{t_0+T} \mathrm{d}t\, \mathrm{e}^{\mathrm{i}\Omega t}\langle d(t)\rangle\right|^2$.

Equation (46) deserves many comments. Note that, in general, there is low-frequency generation, with frequency 2ε for all initial conditions. Only at some particular driving amplitudes this cannot happen: for OIC the low-frequency component can be suppressed when $\sin(2\theta) = 0$; for TIC only when $\cos(2\theta) = 0$. There is always low-frequency generation at any driving amplitude for CTIC. There is odd-harmonics generation at frequencies $(2n-1)\omega$ due to the terms with $R(t)$. These harmonics are generated except when $\cos(2\theta) = 0$ for OIC and except when $\sin(2\theta) = 0$ for TIC. Interestingly enough, CTIN *cannot generate odd harmonics*. Hyper-Raman lines occur at frequencies $2n\omega \pm 2\varepsilon$ and are due to the presence of terms $\sin(2\epsilon t)Q(t)$, $\cos(2\epsilon t)Q(t)$, $\sin(2\epsilon t)P(t)$ or $\cos(2\epsilon t)P(t)$. They are generated except when $\sin 2\theta(v) = 0$ for OIC and except when $\cos 2\theta(v) = 0$ for TIC. They are always present for CTIC.

The presence of odd harmonics and hyper-Raman lines in the dipole expression for the HDTLS is interesting. For a general driven Hamiltonian that possesses the dynamical symmetry $H(x,t) = H(-x, t+\tau/2)$, it has been proven non-perturbatively [41] that the HHG from a Floquet eigenstate consists of only *odd* harmonics. Our Hamiltonian, equation (14), is certainly of this kind since the quantum operator that corresponds to x is σ_x, and therefore, if $\sigma_x \to -\sigma_x$ and $t \to t + \tau/2$, the Hamiltonian in equation (14) remains the same. According to this, a good check for our result can be done by replacing in equation (46) the initial condition $c_a = \cos\theta$, $c_b = \sin\theta$ which corresponds to the initial state being already a Floquet eigenstate (see equation (25)). After doing that, one obtains $\langle d(t)\rangle/\mu = 2R(t)$, which means that this

state only generates odd harmonics, in agreement with the dynamical symmetry arguments developed in the above citation.

The fact that in all HHG experiments using gases (the atomic potential with the laser interaction possesses dynamical symmetry) only odd harmonics are found, shows that only one Floquet eigenstate is excited by the laser pulse, a situation that would be typical for most pulses where the envelope is smooth enough and the OIC applies. As our result (46) shows, for OIC and even when the system has dynamical symmetry (like our HDTLS), it is still possible to generate both hyper-Raman frequencies *and* odd harmonics when the pulse envelope is not smooth. This is the case in our calculation where we have assumed instantaneous turn-on of the driving field. Hyper-Raman lines have also been found in numerical calculations for a double quantum well [42].

Our above result shows that the kind of harmonic present in the spectrum (low frequency, odd harmonics and hyper-Raman lines) is dependent on the initial condition, the two-level energy spacing, the frequency and the driving field amplitude. In addition to this, and in the case of abrupt turn-on, the phase of the driving field should also be important. In this work, we have chosen a driving field of the form $\cos(\omega t)$; for the case $\sin(\omega t)$ with abrupt turn-on, see [35] where it was also found that the initial state of the system affects the generation of odd harmonics and hyper-Raman frequencies.

It is interesting to check our results for the time-dependent dipole moment of the system in the DL regime. As we showed before, in the limit of perfect DL, where $v \to \infty$ or $\tilde{\omega}_0 \to 0$, one gets $\theta = 0, K(t)$ becomes pure real, $Z(t)$ becomes pure imaginary, and therefore $R(t) = Q(t) = P(t) = 0$. The result for the dipole moment is therefore

$$\langle d(t)\rangle/\mu = \cos(2\epsilon t)\,\mathrm{Re}(2c_a c_b^*) - \sin(2\epsilon t)\,\mathrm{Im}(2c_a c_b^*) = 2|c_a c_b|\cos(2\varepsilon t + \gamma), \tag{47}$$

with γ being the phase difference between c_a and c_b. This is the zeroth-order expression in the first-order perturbative results obtained by Delgado and Gomez Llorente [22]. Clearly, in this limit there is *no* HHG. From this it is clear that in the case of a driven two-level system, DL and HHG are at odds; the greater the localization, the smaller the HHG. As one increases the amplitude of the driving field, one would expect the strength of any line in the emission spectrum of this system (except the low-frequency one) to initially increase, then plateau (with fluctuations) and finally decrease as v.

Near the DL regime, we can obtain some expressions and compare them with the perturbative results obtained in other works [15, 20, 22]. For $v > 1$ and $\alpha = \sqrt{\frac{\pi}{32}}\frac{\tilde{\omega}_0}{\sqrt{v}}$, we found that the behaviour of the functions $K(t)$ and $Z(t)$ is

$$\begin{aligned} K(t) &\approx \mathrm{Re}(K(t)) + \mathrm{i}\alpha\kappa(t), \\ Z(t) &\approx \alpha\zeta(t) + \mathrm{i}\,\mathrm{Im}(Z(t)). \end{aligned} \tag{48}$$

Here $\kappa(t)$ and $\zeta(t)$ are periodic functions (even and odd, respectively) with amplitude close to 1. As we have shown before, in this regime, the amplitude of the oscillations in the function $\theta(v)$ is also proportional to α. According to this, and using equation (45), we see that in this regime, $R(t) \propto \alpha$, $Q(t) \propto \alpha$, $P(t) \propto \alpha^2$. We now rewrite equation (46) in a form that makes evident the magnitude of the different terms that contribute to the dipole moment,

$$\begin{aligned} \langle d(t)\rangle \approx\ & [-\alpha\tilde{\theta}\cos(2\epsilon t) + \alpha\tilde{R}(t) + 2\alpha^2\tilde{\theta}\sin(2\epsilon t)\tilde{Q}(t) + 2\alpha^3\tilde{\theta}\cos(2\epsilon t)\tilde{P}(t)](|c_a|^2 - |c_b|^2) \\ & + [\cos(2\epsilon t) - 2\alpha\sin(2\epsilon t)\tilde{Q}(t) + 4\alpha^2\tilde{\theta}\tilde{R}(t) - 2\alpha^2\cos(2\epsilon t)\tilde{P}(t)]\,\mathrm{Re}(2c_a c_b^*) \\ & + [-\sin(2\epsilon t) - 2\alpha\cos(2\epsilon t)\tilde{Q}(t) + 2\alpha^2\sin(2\epsilon t)\tilde{P}(t)]\,\mathrm{Im}(2c_a c_b^*), \end{aligned} \tag{49}$$

where $\tilde{R}(t) = R(t)/\alpha$, $\tilde{Q}(t) = Q(t)/\alpha$, $\tilde{P}(t) = P(t)/\alpha^2$ and $\tilde{\theta} = \theta/\alpha \sim \sin(4v - \pi/4)$. From this expression we can see that in the DL regime OIC generates low frequency and odd-harmonics radiation to second order in α and that hyper-Raman generation is fourth order

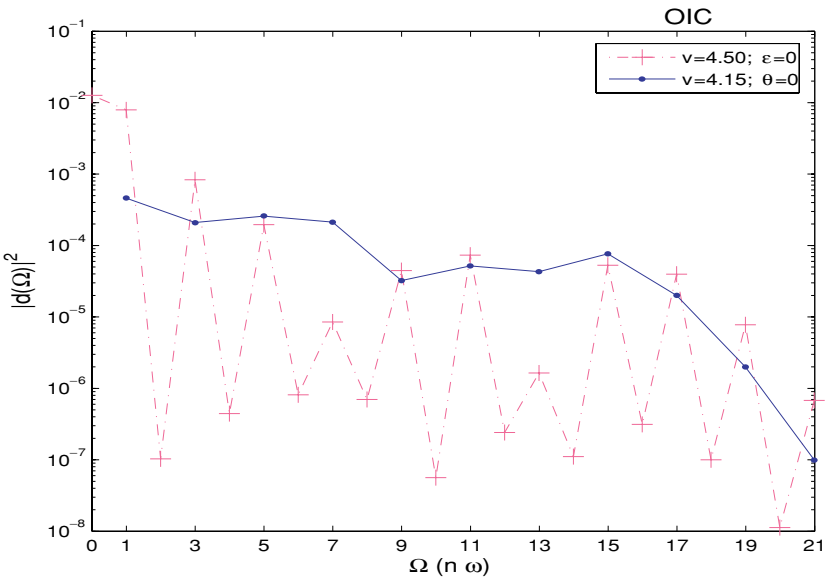

Figure 8. The emission spectrum of the system, for the optical initial condition and for two values of the driving amplitude: $v = 4.5$ corresponds to a DL point and $v = 4.15$ gives $\theta(4.15) = 0$. The Fourier components of $\langle d(t)\rangle$ are connected with a continuous line for better visualization.

in this parameter. For TIC there is strong low-frequency generation independent of any of the parameters of the system (provided we are in DL regime), hyper-Raman generation is second order and odd-harmonic generation is fourth order in α. For CTIC the situation is similar to TIC except that no odd-harmonic radiation is produced.

As mentioned before, from the general expression for the dipole moment, since $\varepsilon = \varepsilon(v)$ and $\theta = \theta(v)$, with successive points where either $\theta(v)$ or $\varepsilon(v)$ vanish, there is a lot of variation in the composition (in terms of odd harmonics and hyper-Raman lines) of the spectrum of this system as a function of the amplitude of the driving field. The interesting exception being the CTIC where odd harmonics are never generated.

In figures 8–10, we show the emission spectrum for three distinct initial conditions (OIC, TIC, CTIC) and for two values of the driving field amplitude. What is common to all these plots is the typical profile of harmonic generation that has been found theoretically and experimentally in different systems. It consists of a plateau where the amplitudes are of similar magnitude (fluctuations are of one to two orders of magnitude typically), followed by a frequency cut-off after which the harmonic amplitudes decay very quickly (exponentially in $n\omega$).

From the structure of the Floquet eigenstates, like the one shown in figure 3, one can see that there is a cut-off in the harmonic components of the eigenstates, which occurs at $N_e = 2v - 1$ (for $v \geqslant 1$). The location of the cut-off in the emission spectrum of the system follows from the location of the cut-off in the eigenstates, since the functions $R(t)$, $Q(t)$, $P(t)$ are second order in the eigenstates components. $R(t)$, $Q(t)$, $P(t)$ therefore have cut-offs at $N_{\rm cut} = 2N_e = 4v - 2$. This is the same cut-off that we expect to see in the emission spectrum of the system.

As we can see in figures 8–10, this result describes quite well the location of the last peak before the components start to decay exponentially. The linear dependence of $N_{\rm cut}$ on the

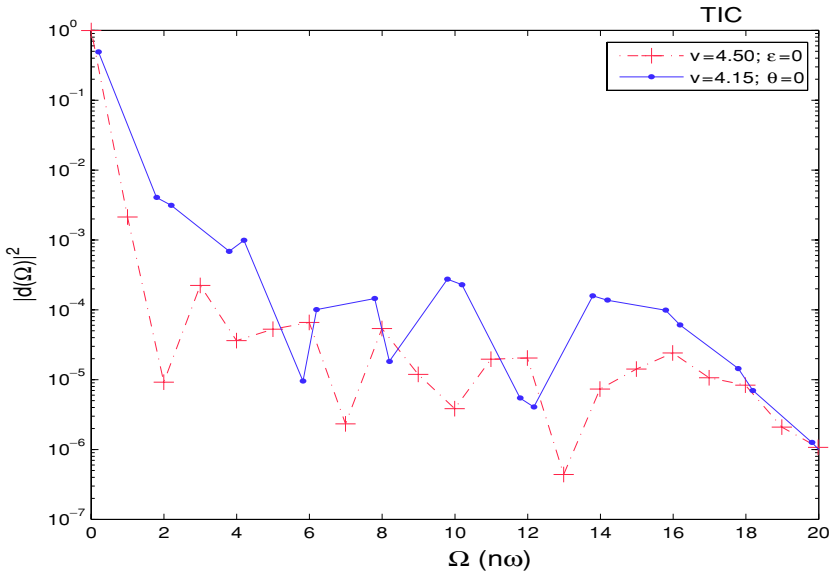

Figure 9. Tunnelling initial condition; other parameters are the same as in figure 8.

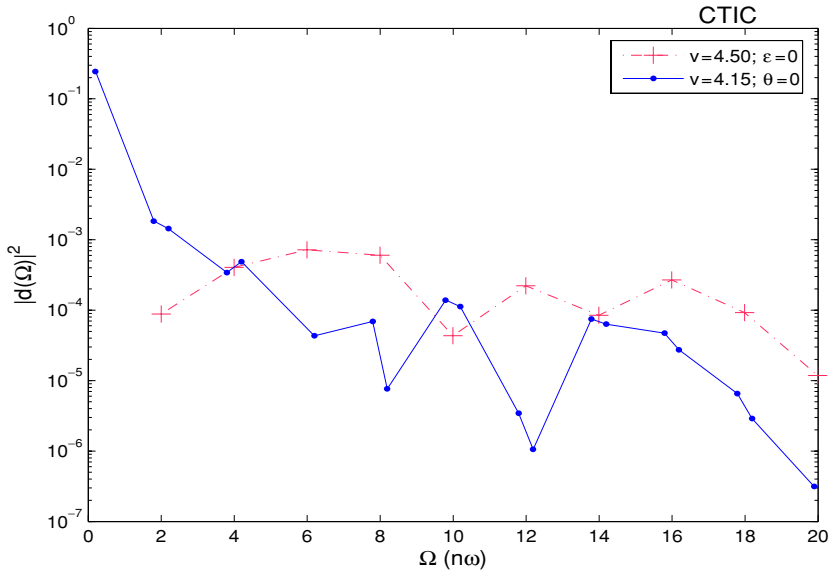

Figure 10. Complex tunnelling initial condition; parameters are the same as in figures 8 and 9.

amplitude of the field implies that $N_{\rm cut} \propto \sqrt{I}$, where I is the intensity of the field. This result is expected for HHG in systems where bound–bound transitions are dominant [46, 47]. For dominant bound–continuum transitions [48], $N_{\rm cut} \propto I$.

In figure 8, we show the emission spectrum for OIC and for two different values of the driving amplitude. For $v = 4.15$ (which gives $\theta \approx 0$), we see, from the first line of equation (49), that one expects no low-frequency component, odd harmonics and no

hyper-Raman lines. For $v = 4.5$ (which gives $\varepsilon \approx 0$), we obtain a strong low-frequency component, strong odd-harmonics components and very weak even-harmonics components that are due to the function $P(t)$ only (since at $\varepsilon = 0$, $\sin(2\epsilon t) = 0$ and therefore $Q(t)$ does not contribute to the spectrum). This is a special case since in general, in this regime, $Q(t)$'s contribution to $|d(\Omega)|^2$ is two orders of magnitude larger than the one from $P(t)$.

In figure 9, we show the emission spectrum for TIC for the same values of v as before. In the $\theta = 0$ case, we can see, from the second line in equation (49), that there is a strong low-frequency component ($\Omega = \pm 2\varepsilon$), no odd harmonics and hyper-Raman lines ($\Omega = 2n \pm 2\varepsilon$). For the case $\varepsilon = 0$, there is a zero-frequency component and also odd and even harmonics of the same magnitude.

Finally, in figure 10, we show the case when the initial condition is CTIC. From the third line in equation (49) we see that, for the case $\theta = 0$, we should get a strong low-frequency component and hyper-Raman lines. For the $\varepsilon = 0$ case, there is no static component, only even harmonics.

For the characteristic plateau of HHG to appear, it was shown [30] that $v \geqslant \sqrt{\tilde{\omega}_0}$. In this region we have found numerically that $\cos(2\theta) \neq 0$, which means that in OIC, overall, the odd harmonics are much more stable with respect to changes in the driving amplitude than the hyper-Raman lines, which as a whole, do fluctuate with v (following the behaviour of $\sin(2\theta)$). As one approaches the DL regime, the odd harmonics will dominate the spectrum for OIC (which is the initial condition most easily obtained experimentally). It is easy to derive an estimate for the conditions under which odd harmonics will dominate over hyper-Raman lines for OIC. For that we take $\alpha \geqslant 0.1$, so that there is at least one order of magnitude difference in their contributions to equation (49). From $\alpha = \sqrt{\frac{\pi}{32}}\frac{\tilde{\omega}_0}{\sqrt{v}}$, one gets the estimate

$$v \gtrsim 10\tilde{\omega}_0^2.$$

When this condition is satisfied, odd harmonics will clearly dominate the spectrum in the OIC.

Determining the harmonic generation when the system interacts with a pulse with a smooth turn-on envelope is a simple procedure. It involves finding the projection of the initial state onto the Floquet eigenstates corresponding to the limit $v \to 0$. After this, one determines how each Floquet eigenstate evolves (adiabatically) with an increasing amplitude of the pulse. Finally, when the pulse has reached its maximum amplitude, one finds the harmonic generation due to this stationary state, by projecting back onto the basis $\{|a\rangle, |b\rangle\}$ (which gives c_a and c_b) and then inserting this into equation (46). For corrections to this adiabatic approximation, one can follow the work in [27].

6. Summary and conclusions

In this work, we used a complete Floquet–Green operator formalism for the analytical solution of a harmonically driven two-level system. From this operator, we were able to completely solve the system and obtain the quasi-energies and the eigenstates in terms of continued fractions.

We were able to obtain analytical expressions for the components of the Floquet eigenstates and from them we constructed the time-evolution operator of this system. The structure of the eigenstates revealed a characteristic pattern, with an 'irregular' region where the components are sensitive to small changes in v, change sign and have zeros, and a 'regular' region where the components depend less sensitively on v, and decay exponentially with the frequency $n\omega$. The cut-off frequency that divides the two regions and gives the position of the largest Floquet component of the eigenstates is proportional to the driving field strength v, $N_e = 2v - 1$, a result that is valid for any $\tilde{\omega}_0$ (provided $v > \sqrt{\tilde{\omega}_0}$).

From the time-evolution operator, we were able to study dynamic localization, which is one of the important features of this Hamiltonian. It is known that DL is obtained at values of the driving field strength for which the quasi-energies vanish. In quantum computation, this localization mechanism can be of great importance for controlling the state of a q-bit (e.g. a double quantum well), since the amount of tunnelling of an electron between two adjacent wells can be varied with the intensity of the driving field. In this work, we obtained a correlation between the DL points and the maxima of the quantity $\theta(v)$ that describes the Floquet eigenstates of the system. Also, the value of the function $\cos^2(2\theta(v))$, at its lowest minima, was found to give a good approximation to the degree of localization of the system at the corresponding DL points. Interestingly, these points appear in pairs with similar degrees of localization corresponding to each pair. We also found the approximate equation

$$v \approx \frac{\pi \tilde{\omega}_0^2}{8(1 - P_l)},$$

which, at the DL points, relates the degree of localization P_l, with the energy level difference ω_0, and the amplitude v of the driving field (all quantities in units of $\hbar\omega$). This equation can be used to easily estimate the amount of localization achievable in this system for a given set of parameters.

For the study of HHG in this system, we calculated the expected value of the dipole moment which revealed that the emission spectrum, in general, can contain low-frequency components, odd harmonics and hyper-Raman lines. The particular components and their amplitudes depend strongly on the initial state of the system and on the specific driving field amplitude. We found that there exists an initial condition (CTIC) of the driven two-level system for which no odd harmonics can be generated at any driving field strength. For each one of the 'pure' initial conditions, namely OIC, TIC or CTIC, the driving amplitudes where $\theta(v) = 0$ produce either only hyper-Raman lines or only odd harmonics, depending on the particular initial condition. For all other driving amplitudes, there will be in general generation of both kinds of frequencies (except for CTIC). When the initial condition is a Floquet eigenstate (which is equivalent to the smooth turn-on case for OIC), we found that only odd harmonics are generated, a result that is expected from the dynamical symmetry of the Hamiltonian. In general, we can say that the emission spectrum of the driven two-level system is sensitive to different parameters, such as the initial preparation, the amplitude of the driving and its phase.

For small values of α, but still not deep into the DL regime, we obtained an equation which directly relates the emission spectrum with the localization parameter α. We showed the different magnitude of the terms that give low frequency, odd harmonics and hyper-Raman lines (which become even harmonics at the degeneracy points). In the optical initial condition (OIC), we found that odd-harmonics generation is stronger, the hyper-Raman lines are weaker and even nonexistent for particular values of the driving field amplitude (when $\theta(v) = 0$). For tunnelling initial condition (TIC), hyper-Raman lines dominate, except at the DL points ($\varepsilon = 0$), where even and odd harmonics have approximately the same amplitude. For complex tunnelling initial condition (CTIC), no odd harmonics are generated.

Well inside the dynamic localization regime, odd harmonics are exclusively generated in the optical initial condition and hyper-Raman lines only occur in the tunnelling initial conditions (TIC and CTIC). In this regime of high localization, HHG decreases with decreasing α, a situation that clearly places both effects on opposite sides of the parameter space, although with significant overlap between them. In general, for a driven two-level system, the strongest HHG should occur for higher values of $\tilde{\omega}_0$ and for driving amplitudes $v \lesssim 10\tilde{\omega}_0^2$ (for $\alpha > 0.1$). For strong DL, smaller values of $\tilde{\omega}_0$ and/or bigger values of v are required, $v \gtrsim 10\tilde{\omega}_0^2$

(for $\alpha < 0.1$). *Strong* HHG in a two-level system is an eminently non-linear, non-perturbative phenomenon.

The HDTLS has been shown to be useful in understanding basic features of the interaction of light with matter, even though, clearly, the full complexity of the general processes in atoms and molecules cannot be accounted for with this model. The model predicts an emission spectrum with a plateau and a cut-off frequency, whose location depends on the square root of the intensity of the driving field (since $N_{\mathrm{cut}} \propto v \propto E \propto \sqrt{I}$). Such dependence has been found in systems where bound–bound transitions account for most of the HHG [46, 49]. For the case of charge-resonant states of odd-charge molecular ions, it has also been argued [20] that this simple two-level model can account for the behaviour of these molecules in a strong laser pulse. A square-root dependence of the cut-off frequency with the intensity of the laser field can be found in several experiments [45], a fact that is characteristic of a driven two-level system and which might point in the direction of an effective two-level dynamics for some systems [30].

HHG and DL are two major features of a driven two-level system with a great range of applications in atomic and solid-state systems where coherent sources of radiation and control of quantum states are sought. With this work we have established a connection between these two phenomena and provided new results and a more detailed description of this system.

Acknowledgments

The author would like to thank Professor L E Reichl for her support. This work was partly funded by the The Robert A Welch Foundation (grant no F-1051), the Engineering Research Program of the Office of Basic Energy Sciences at the US Department of Energy (grant no DE-FG03-94ER14465) and the US Navy Office of Naval Research (grant no N00014-03-1-0639).

Appendix. Components of the Floquet eigenstates

From the definition of the Floquet–Green operator, we have shown in equation (10) that the residue of the function $\mathcal{G}_{0,0}(E)$ at a pole $E = \varepsilon + p$ is the operator (2×2 matrix) $\left|\phi_p^{\varepsilon}\right\rangle\left\langle\phi_p^{\varepsilon}\right|$, where $\left|\phi_p^{\varepsilon}\right\rangle$ is the pth Fourier component of the Floquet eigenstate corresponding to the quasi-energy ε. If we write $\left|\phi_p^{\varepsilon}\right\rangle \equiv K_p|a\rangle + Z_p|b\rangle$, then, in principle, from the residue (a matrix) of $\mathcal{G}_{0,0}$ we could determine the components K_p, Z_p. This is only true, however, provided the residue does not turn out to be a diagonal matrix. Unfortunately, this is the case for the system we are considering, since, as we mentioned before, $G_{0,0}(E)$ *is* a diagonal matrix ($V_{\mathrm{eff}}(E)$ is diagonal), and therefore its residue only gives us information about $|K_p|^2$ and $|Z_p|^2$. From equation (8) we can see that the off-diagonal components $G_{m,0}$ can give us the needed components:

$$\mathcal{G}_{m,0}(E) = \sum_{\gamma,p} \frac{1}{E - \varepsilon_\gamma - p} \left|\phi_{m+p}^{\varepsilon_\gamma}\right\rangle\left\langle\phi_p^{\varepsilon_\gamma}\right|. \tag{A.1}$$

From this we get that at the pole $E = \varepsilon_\gamma$ (and therefore $p = 0$), the residue is $\left|\phi_m^{\varepsilon_\gamma}\right\rangle\left\langle\phi_0^{\varepsilon_\gamma}\right|$. From all these residues for all values of m, one could therefore extract all the eigenvector components $\left|\phi_m^{\varepsilon_\gamma}\right\rangle$.

The $\mathcal{G}_{m,0}$ operators can be obtained from $\mathcal{G}_{0,0}$, as it was shown in [26]. The result is

$$\begin{aligned}
&\mathcal{G}_{1,0} = F_0^+ \mathcal{G}_{0,0},\\
&\mathcal{G}_{2,0} = F_1^+ \mathcal{G}_{1,0} = F_1^+ F_0^+ \mathcal{G}_{0,0},\\
&\vdots\\
&\mathcal{G}_{m,0} = F_{m-1}^+ \mathcal{G}_{m-1,0} = \prod_{j=0}^{m-1} F_j^+ \mathcal{G}_{0,0}(E), \qquad \text{for} \quad m > 0,
\end{aligned} \tag{A.2}$$

and where (showing explicitly the energy dependence)

$$F_j^+(E) \equiv (V\mathcal{F}_{j,0}(E))^{-1} V = V^{-1} V_{\text{eff}}^+(E+j) = \begin{bmatrix} 0 & \frac{1}{v} v_b^+(E+j) \\ \frac{1}{v} v_a^+(E+j) & 0 \end{bmatrix}, \tag{A.3}$$

and similarly,

$$\mathcal{G}_{-m,0}(E) = \mathcal{F}_{-m+1}^- G_{-m+1,0} = \prod_{j=0}^{m-1} \mathcal{F}_{-j}^- G_{0,0}, \qquad \text{for} \quad m > 0, \tag{A.4}$$

with

$$F_{-j}^-(E) \equiv (V\mathcal{F}_{-j,0}(E))^{-1} V = V^{-1} V_{\text{eff}}^-(E-j) \quad = \begin{bmatrix} 0 & \frac{1}{v} v_b^-(E-j) \\ \frac{1}{v} v_a^-(E-j) & 0 \end{bmatrix}. \tag{A.5}$$

It is not difficult to show using equations (A.1), (A.2) and (A.4) that

$$\left|\phi_{m+1}^{\varepsilon_\gamma}\right\rangle = F_m^+(\varepsilon_\gamma)\left|\phi_m^{\varepsilon_\gamma}\right\rangle$$

and

$$\left|\phi_{m-1}^{\varepsilon_\gamma}\right\rangle = F_m^-(\varepsilon_\gamma)\left|\phi_m^{\varepsilon_\gamma}\right\rangle, \tag{A.6}$$

with $\varepsilon_\gamma = \pm\varepsilon$.

As we already mentioned, at $E = \varepsilon$ the residue of $G_{0,0}(E)$ is proportional to $|b\rangle$ and at $E = -\varepsilon$ the residue is proportional to $|a\rangle$. From this, and using equation (A.6) together with equations (A.3) and (A.5), we can write explicitly the two Floquet eigenstates of this system:

$$\begin{aligned}
|\phi^{-\varepsilon}(t)\rangle = N\Bigg[&\cdots + \frac{\mathrm{e}^{2\mathrm{i}\omega t}}{v^2} v_b^-(-\varepsilon-1) v_a^-(-\varepsilon)|a\rangle + \frac{\mathrm{e}^{\mathrm{i}\omega t}}{v} v_a^-(-\varepsilon)|b\rangle + |a\rangle \\
&+ \frac{\mathrm{e}^{-\mathrm{i}\omega t}}{v} v_a^+(-\varepsilon)|b\rangle + \frac{\mathrm{e}^{-2\mathrm{i}\omega t}}{v^2} v_b^+(-\varepsilon+1) v_a^+(-\varepsilon)|a\rangle + \cdots \Bigg],\\
|\phi^{\varepsilon}(t)\rangle = N\Bigg[&\cdots + \frac{\mathrm{e}^{2\mathrm{i}\omega t}}{v^2} v_a^-(\varepsilon-1) v_b^-(\varepsilon)|b\rangle + \frac{\mathrm{e}^{\mathrm{i}\omega t}}{v} v_b^-(\varepsilon)|a\rangle + |b\rangle \\
&+ \frac{\mathrm{e}^{-\mathrm{i}\omega t}}{v} v_b^+(\varepsilon)|a\rangle + \frac{\mathrm{e}^{-2\mathrm{i}\omega t}}{v^2} v_a^+(\varepsilon+1) v_b^+(\varepsilon)|b\rangle + \cdots \Bigg],
\end{aligned} \tag{A.7}$$

with N being a normalization constant. If we use the symmetry relations, $v_b^-(-E) = -v_a^+(E)$ and $v_b^+(-E) = -v_a^-(E)$, we can write these two eigenstates in a more compact way,

$$\begin{aligned}
|\phi^{-\varepsilon}(t)\rangle &= K(t)|a\rangle + Z(t)|b\rangle,\\
|\phi^{\varepsilon}(t)\rangle &= -Z(t)^*|a\rangle + K(t)^*|b\rangle,
\end{aligned} \tag{A.8}$$

with

$$
\begin{aligned}
K(t) &= N\Bigg(\cdots + \frac{\mathrm{e}^{4\mathrm{i}\omega t}}{v^4} v_b^-(-\varepsilon-3) v_a^-(-\varepsilon-2) v_b^-(-\varepsilon-1) v_a^-(-\varepsilon) \\
&\quad + \frac{\mathrm{e}^{2\mathrm{i}\omega t}}{v^2} v_b^-(-\varepsilon-1) v_a^-(-\varepsilon) + 1 + \frac{\mathrm{e}^{-2\mathrm{i}\omega t}}{v^2} v_b^+(-\varepsilon+1) v_a^+(-\varepsilon) \\
&\quad + \frac{\mathrm{e}^{-4\mathrm{i}\omega t}}{v^4} v_b^+(-\varepsilon+3) v_a^+(-\varepsilon+2) v_b^+(-\varepsilon+1) v_a^+(-\varepsilon) \Bigg) \\
&= N\left[\sum_{n=-\infty}^{\infty} \mathrm{e}^{-2\mathrm{i}n\omega t} K_{2n}(-\varepsilon) \right], \qquad \text{(A.9)} \\
Z(t) &= N\Bigg[\cdots \frac{\mathrm{e}^{3\mathrm{i}\omega t}}{v^3} v_a^-(-\varepsilon-2) v_b^-(\varepsilon-1) v_a^-(-\varepsilon) + \frac{\mathrm{e}^{\mathrm{i}\omega t}}{v} v_a^-(-\varepsilon) \\
&\quad + \frac{\mathrm{e}^{-\mathrm{i}\omega t}}{v} v_a^+(-\varepsilon) + \frac{\mathrm{e}^{-3\mathrm{i}\omega t}}{v^3} v_a^+(-\varepsilon+2) v_b^+(-\varepsilon+1) v_a^+(-\varepsilon) \cdots \Bigg] \\
&= N\left[\sum_{n=-\infty}^{\infty} \mathrm{e}^{-\mathrm{i}(2n-1)\omega t} Z_{2n-1}(-\varepsilon) \right],
\end{aligned}
$$

where N is a normalization constant so that $|K(t)|^2 + |Z(t)|^2 = 1$, and we have

$$
\begin{aligned}
K_{2n}(-\varepsilon) &= \begin{cases} 1, & \text{for } n = 0, \\ \displaystyle\prod_{j=1}^{|n|} \frac{1}{v^2} v_b^{\mathrm{sg}(n)}(-\varepsilon + \mathrm{sg}(n)(2j-1)) v_a^{\mathrm{sg}(n)}(-\varepsilon + \mathrm{sg}(n)(2j-2))), & \text{for } |n| > 0, \end{cases} \\
Z_{2n+1}(-\varepsilon) &= \begin{cases} \dfrac{1}{v} v_a^+(-\varepsilon+2n) K_{2n}(-\varepsilon), & \text{for } 2n+1 > 0, \\ \dfrac{1}{v} v_a^-(-\varepsilon+2n+2) K_{2n+2}(-\varepsilon), & \text{for } 2n+1 < 0, \end{cases}
\end{aligned} \qquad \text{(A.10)}
$$

and we used $\mathrm{sg}(x) \equiv x/|x|$.

References

[1] Eden J G 2004 *Prog. Quantum Electron.* **28** 197
[2] Platero G and Aguado R 2004 *Phys. Rep.* **395** 1
[3] Kohler S, Lehmann J and Hänggi P 2005 *Phys. Rep.* **406** 379
[4] Cannon J R 1984 *The One-Dimensional Heat Equation (Encyclopedia of Mathematics and its Applications* vol 23*)* (Cambridge: Cambridge University Press)
[5] Großmann F, Dittrich T, Jung P and Hänggi P 1991 *Phys. Rev. Lett.* **67** 516
[6] Meystre P 1992 *Opt. Commun.* **90** 41
[7] Shore B W 1990 *The Theory of Coherent Atomic Excitation* (New York: Wiley)
[8] Autler S H and Townes C H 1955 *Phys. Rev.* **100** 703
[9] Shirley J H 1965 *Phys. Rev.* B **138** 979
[10] Ruyten W M 1990 *Phys. Rev.* A **42** 4226
[11] Stenholm S 1972 *J. Phys. B: At. Mol. Phys.* **5** 878
[12] Agarwal G S and Nayak N 1986 *J. Phys. B: At. Mol. Phys.* **19** 3385
[13] Zhao X G 1994 *Phys. Rev.* B **49** 16 753
[14] Wang H 1996 *Phys. Lett.* A **217** 225
[15] Dakhnovskii Y and Bavli R 1993 *Phys. Rev.* B **48** 11020
[16] Sacchetti A 2001 *J. Phys. A: Math. Gen.* **34** 10293
[17] Frasca M 2003 *Phys. Rev.* B **68** 165315

[18] Barata J C A and Wreszinski W F 2000 *Phys. Rev. Lett.* **84** 2112
[19] Dunlap D H and Kenkre V M 1986 *Phys. Rev.* B **34** 3625
[20] Ivanov M Yu and Corkum P B 1993 *Phys. Rev.* A **48** 580
[21] Santana A, Gomez Llorente J M and Delgado V 2001 *J. Phys. B: At. Mol. Opt. Phys.* **34** 2371
[22] Delgado V and Gomez Llorente J M 2000 *J. Phys. B: At. Mol. Opt. Phys.* **33** 5403
[23] Zel'dovich B Ya 1967 *Sov. Phys.—JETP* **24** 1006
[24] Sambe H 1972 *Phys. Rev.* A **7** 2203
[25] Faisal F H M 1989 *Comput. Phys. Rep.* **9** 55
[26] Martinez D F 2003 *J. Phys. A: Math. Gen.* **36** 9827
[27] Drese K and Holthaus M 1999 *Eur. Phys. J.* D **5** 119
[28] Shultz P A, Rivera P H and Studart N 2002 *Phys. Rev.* B **66** 195310
[29] Martinez D F and Reichl L E 2001 *Phys. Rev.* B **64** 245315
[30] Kaplan A E and Shkolnikov P L 1994 *Phys. Rev.* A **49** 1275
[31] Dimitrovski D, Solov'ev E A and Briggs J S 2004 *Phys. Rev. Lett.* **93** 083003
[32] Gush R and Gush H P 1972 *Phys. Rev.* A **6** 129
[33] Villas-Bôas J M, Zhang W, Ulloa S E, Rivera P H and Studart N 2002 *Phys. Rev.* B **66** 085325
[34] Sundaram B and Milonni P W 1990 *Phys. Rev.* A **41** R6571
[35] Gauthey F I, Keitel C H, Knight P L and Maquet A 1995 *Phys. Rev.* A **52** 525
[36] Gauthey F I, Keitel C H, Knight P L and Maquet A 1997 *Phys. Rev.* A **55** 615
Gauthey F I, Garraway B M and Knight P L 1997 *Phys. Rev.* A **56** 3093
[37] Pons M L, Taïeb R and Maquet A 1996 *Phys. Rev.* A **54** 3634
[38] Abramowitz M and Stegun I A 1965 *Handbook of Mathematical Functions* (New York: Dover) p 497
[39] Milfeld K F and Wyatt R E 1983 *Phys. Rev.* A **27** 72
[40] Creffield C E 2004 *Europhys. Lett.* **66** 631
[41] Ben-Tal N, Moiseyev N and Beswick A 1993 *J. Phys. B: At. Mol. Opt. Phys.* **26** 3017
Alon O E, Averbukh V and Moiseyev N 1998 *Phys. Rev. Lett.* **80** 3743
[42] Bavli R and Metiu H 1993 *Phys. Rev.* A **47** 3299
[43] Wang H, Freire V N and Zhao X G 1998 *Phys. Rev.* A **58** 1531
[44] Protopapas M, Keitel C H and Knight P L 1997 *Rep. Prog. Phys.* **60** 389 and references therein
[45] L'Huillier A, Schafer K J and Kulander K C 1991 *J. Phys. B: At. Mol. Opt. Phys.* **24** 3315
L'Huillier A, Schafer K J and Kulander K C 1991 *Phys. Rev. Lett.* **66** 2200
L'Huillier A, Lompré L-A, Mainfray G and Manus C 1992 *Atoms in Intense Laser Field* ed M Gavrila (Boston, MA: Academic) p 139
[46] Averbukh V, Alon O E and Moiseyev N 2001 *Phys. Rev.* A **64** 033411
[47] Žďánská P, Averbukh V and Moiseyev N 2003 *J. Chem. Phys.* **118** 8726
[48] Corkum P B 1993 *Phys. Rev. Lett.* **71** 1994
Kulander K C, Schafer K J and Krause J L 1993 *Super-Intense Laser-Atom Physics (NATO Advanced Study Institute, Series B: Physics* vol 316*)* ed B Pirax, A L'Huillier and K Rzewski (New York: Plenum) p 95
Lewenstein M, Balcou Ph, Ivanov M Yu, L'Huillier A and Corkum P B 1994 *Phys. Rev.* A **49** 2117
[49] Gupta A K, Alon O E and Moiseyev N 2003 *Phys. Rev.* B **68** 205101